

Origin of fast electrons in catalytic hydrogen oxidation over platinum

Sergey N. Maximoff^{1, a)} and Martin Head-Gordon^{1, 2}

¹⁾*Department of Chemistry, University of California, Berkeley, CA 94720, USA*

²⁾*Chemical Sciences Division, Lawrence Berkeley National Laboratory, Berkeley, CA 94720, USA*

Adsorption of small molecules and chemical reactions at metal surfaces always excite low energy electron-hole pairs since the electron-hole pair excitations are gapless. In an example catalytic process, H_2 oxidation by O_2 into H_2O over a platinum surface Pt(111), this report explains that a different mechanism must also excite a non-equilibrium population of fast electrons, which arise as charged surface intermediates develop and then discharge during rapid electron transfer events. The empirical evidence and quantum chemistry calculations further reveal that the transition states in the H_2 oxidation are the lowest threshold configurations for changing the charge of the negatively charged surface intermediates as in, e.g., $[\text{O}^- + \text{H}^-] \rightleftharpoons [\text{O}^- + \text{H} + e]^\ddagger \rightleftharpoons [2e + \text{OH}^-]$ and $[\text{OH}^- + \text{H}^-] \rightleftharpoons [\text{OH}^- + \text{H} + e]^\ddagger \rightleftharpoons [2e + \text{H}_2\text{O}]$. The activation energies correspond to the lowest thresholds for the accessible scattering channels that circumvent the repulsion between the negatively charged surface intermediates by detaching an electron from the intermediates into the metal. This picture should also apply to other catalytic chemical reactions on metal surfaces that proceed through formation of charged intermediates and their consequent discharge.

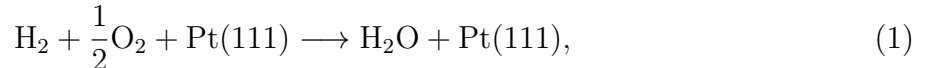
^{a)}Electronic mail: SNMaximoff@gmail.com

I. INTRODUCTION

Evidence has been mounting^{1–10} that exothermic redox chemical reactions at high workfunction surfaces of electron-rich noble and late transition metals may excite electrons that propagate for about a few nanometers into the metal at kinetic energies $\gtrsim 0.5 - 1.2$ eV, but below the workfunction barrier for electron ejection from the metal ($4.3 - 5.9$ eV¹¹). If real, these excitations must propagate inside the metal rather than in a vacuum, and therefore are tricky to probe directly in experiments. Claims of their detection are based on Schottky diode experiments (figs. 1(a) and 1(b)). These experiments aim to register these excitations indirectly as a zero voltage bias electric current through high workfunction metal film/semiconductor Schottky diodes with $0.5 - 1.2$ eV Schottky barriers^{1,6,12} during adsorption-desorption or reactive adsorption-desorption of molecules or atoms at the interface between the gas and the diode at pressures ranging from ultra high vacuum (UHV) to pressures on the order of one bar¹. A catalytic Schottky diode is a thin film of a catalytic metal that joins a thicker film of a semiconductor so that the Schottky barrier at the interface of the metal and semiconductor passes the current of thermal electrons in the direction from the semiconductor to the metal but not in the opposite direction.

The interpretation of a meaning for this zero-bias current depends on the following hypothesis. If adsorption-desorption, or reactive adsorption-desorption at the interface between the metal and the gas invokes electronic excitations of energy in excess of the Schottky barrier height, then some of these excitations propagate through the metal, surpass the Schottky barrier, and contribute discernibly to a zero bias current. The current flows through the diode from the metal-gas interface to the semiconductor and it does not originate from other sources of zero voltage bias currents, such as the thermoelectric effect in response to a temperature gradient across the semiconductor. Under this hypothesis, the source of the zero-bias current must reside and should be sought within the gas-metal interface.

Ref. 1 has been the first to report that an exothermic catalytic chemical process,



over a 5 nm thick Pt film in Pt/n-TiO₂ diode with the Schottky barrier of $1.1 - 1.2$ eV induces a zero-bias current. Equation (1) has the reaction heat of $\Delta H_{\text{H}_2\text{O}} = -2.51$ eV¹³, and it proceeds at the reaction rate $R(\text{H}_2\text{O}) = k(T)p_{\text{H}_2}$ at the constant partial pressures $p_{\text{H}_2} = 6$ Torr and $p_{\text{O}_2} = 760$ Torr in the temperature range $298 - 373$ K where

$k(T) \propto \exp(-E^\ddagger(\text{H}_2\text{O})/kT)$ and the activation barrier is $E^\ddagger(\text{H}_2\text{O}) = 0.32 - 0.33$ eV. The current through the diode that originates at the gas-metal interface, $I_c = Y_c R(\text{H}_2\text{O})$, has the apparent yield, $Y_c(\text{H}_2\text{O}) = (1.1 \pm 0.1) \cdot 10^{-4}$. Furthermore, Ref. 8 indicates that this current arises because of eq. (1) rather than other processes intrinsic to the Schottky diode. Similar phenomena have also been seen in catalytic CO oxidation by O_2 ^{14,15} or by NO ⁷ at platinum and palladium surfaces.

This report is a theoretical investigation into the basic question: ‘How can eq. (1), and similar chemical reactions, contribute to the current measured in the Schottky diode experiments?’ Reactive or non-reactive adsorption-desorption at metal surfaces has long been known to involve energy transfer between localized molecular degrees of freedom and delocalized metal electrons in an irremovable way, thus pushing chemistry at metal surfaces away from the left end towards the right end of the ‘adiabatic→nonadiabatic’ spectrum^{12,16}. However, the latter has an essentially multifactorial structure, which is a consequence of the existence of very different types of mechanisms of energy transfer between the metal electrons and molecules at a gas-metal interface. These mechanisms are either of the electron-hole pair type or fast electron type (as it will be called).

The qualitative nature of an electron-hole pair mechanism does not depend on anything about an adsorbed molecule except that its localized charge distribution is a source of the time-dependent potential that does not bind electrons at the metal surface. This potential must excite electron-hole pairs, which are low-energy electronic excitations of a bulk metal, since (i) the electron-hole pair spectrum is gapless, and (ii) the excitation energy-dependent coupling constant between the potential and delocalized electron-hole pairs grows strong and singular at low energies (Anderson’s orthogonality catastrophe, see, e.g., reviews^{17,18} and references therein). These two conditions apply stably in normal metals, and suffice to ensure a high rate of production of low-energy electron-hole pairs in response to the motion of an adsorbate. The rate of electron-hole pair excitations falls off quickly with the excitation energy. Details of the electron-hole pair mechanism are modified if an adsorbate has internal electronic degrees of freedom, which couple resonantly to the electron-hole-pairs around a minimum on the ground state adiabatic potential, but in essence remain the same¹⁹.

The electron-hole pair mechanism is a hallmark of a metal’s low-energy response to a localized perturbation, but it does not explain the emergence in eq. (1) of excitations whose energy well exceeds the typical energy of an electron-hole pair^{20–22}. A key to the resolution

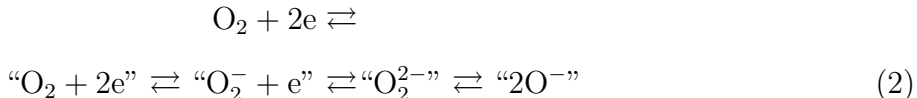
of this apparent paradox lies in the fast electron type of mechanism, which does not depend on anything about the metal except its being a reservoir of delocalized electrons, but instead depends on the capacity of the internal molecular degrees of freedom to accept or donate metal electrons. The molecular excitation spectrum includes both discrete and continuum branches. The discrete excitations bear labels of bound electronic and rovibrational modes, while the continuum branches arise as translational excitations of internally excited molecular fragments. Thresholds, which correspond to vanishing kinetic energy of translationally excited fragments, link the discrete and continuum branches of the spectrum. A molecule in the midst of a reservoir of electrons can localize electrons in bound states if the total energy of the molecule and electrons is below the minimum accessible electron detachment threshold. When the total energy exceeds this threshold, the molecule becomes a source of translationally excited electrons. At the metal-gas interface, such electrons are subject to a time-dependent electric field, which is the response of the metal surface to the molecular charge distribution. This electric field performs work on the electrons in the molecular electron detachment continuum, and the latter, in turn, couples to the continuum of the conduction band electrons in the metal. Thus fast electrons arise as excitations intrinsic to the free-electron branches of the molecular continuum spectrum. Since these fast electrons are not intrinsic excitations in a normal metal, they must eventually lose their energy while giving rise to showers of electron-hole pairs, low energy phonons, and radiation. Thus, the fast electron mechanism depends on four properties: (i) the molecular excitation spectrum features electron detachment thresholds; (ii) electron detachment branches of the molecular excitation spectrum hybridize with the conduction band continuum of the metal; (iii) the metal is a reservoir of electrons and the gas-metal interface can support directional flux of electrons; (iv) the electric field at the metal-gas interface accelerates electrons in the molecular continuum but not the localized molecular electrons. These properties are stable.

It is not at all new that internal degrees of freedom of atoms and molecules play a role in energy flow between metal electrons and molecules through transient retention of metal electrons by the internal degrees of freedom^{16,19}. For instance, Refs. 5 and 23 bring up the significance of temporary molecular anions in energy relaxation in molecular scattering against metal surfaces. Refs. 22, 24, and 25 discuss how transient charge transfer between adsorbates and metal surfaces facilitates rovibrational energy relaxation. Ref. 26 explains how molecular degrees of freedom give rise to fast electrons in CO oxidation on Pt(111).

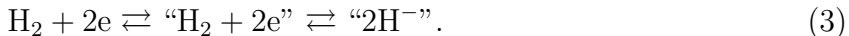
This report argues that the nature of the microscopic events underlying eq. (1) is such that fast electrons must emerge ubiquitously, and these events have the same origin as those discussed in the context of CO oxidation on Pt(111)²⁶.

Section II translates on a heuristic level the problem of electronic excitations underlying eq. (1) to the language of scattering theory, which is convenient for describing the excitation events in eq. (1). A default assumption, both widely understood and convenient, in chemical dynamics is the adiabatic representation in a basis of Born-Oppenheimer states at fixed nuclear positions. However, the main theme of this report is a qualitative picture of attachment and detachment of metal electrons by the interface during a catalytic chemical reaction such as eq. (1). The adiabatic representation is unnatural near thresholds for electron detachment where a fraction of internal energy becomes the kinetic energy of electrons, electrons can be very slow, and there is no good general reason to separate the motion in slower nuclear and faster electronic degrees of freedom. For that reason, the constructs of adiabatic representation have been avoided in scattering theory, where the language of channels²⁷ is more appropriate. Unlike the adiabatic representation, the channel representation does not localize chemical events and requires an additional localization structure. This report takes a position that the qualitative discussion of surface chemistry has to begin in the framework of scattering channels and in terms of their localization to a region of an interface.

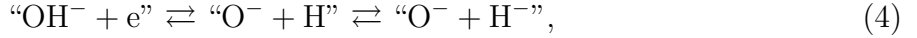
Section III examines the empirical evidence and uses quantum chemistry models to describe the channels that contribute to the electron attachment-detachment events in eq. (1). The products, $(\text{H}_2\text{O})_n$, and the reactants, H_2 and O_2 , are electroneutral, but eq. (1) involves anionic intermediates at the metal-gas interface. Since the chemical process in eq. (1) is catalytic, the anionic intermediates are not permanent, and, by charge conservation, an intermittent charge flux from and to the interface is inevitable. The origin of the charge flux from the metal to the interface is the exothermic dissociative electron attachment to the H_2 and O_2 molecules that adsorb from the thermal gas through events such as



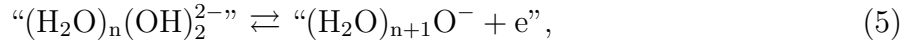
and



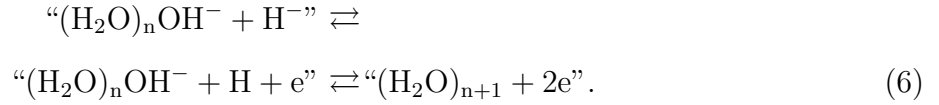
Here, the notation “ A ” reads as ‘a chemical entity within the interface that has an appearance of an isolated A .’ The origin of the charge transfer from the interface to the metal is the exothermic but activated electron detachment into the metal’s conduction band from high energy negatively charged intermediates, which emerge in reactions such as hydroxyl dissociation and association,



disproportionation of “ $(\text{H}_2\text{O})_n\text{O}^-$ ”,



dissociation of “ H_2O ” or association of OH^- and H^- ,



For the associative electron detachment events to proceed, the total energy of the colliding anionic intermediates on the left-hand sides of eq. (6) and eq. (5) must exceed the minimum accessible threshold for electron detachment into the conduction band of the metal from the interface (the middle terms in eq. (4), eq. (5), eq. (6)), as an extended many-body system. These minimum thresholds are the activation barriers for the electron detachment events. The energy in excess of the thresholds distributes over the translational degrees of freedom of the electrons and molecules departing the interface and the internal degrees of freedom of the interface. Some of the electron detachment channels at the energies above the lowest accessible threshold for electron detachment couple to the channels that include the low internal energy neutral molecules and fast metal electrons. Section IV concludes the report.

II. PRELIMINARY EXAMINATION

There is the thermal gas of H_2 , O_2 , and H_2O molecules (fig. 1(a)). There is platinum metal whose conduction electrons (e) form a pool of high density degenerate electron liquid moving in the background of the crystal field of the heavy, nearly harmonic Pt ions in the *fcc* crystal. To the left of the gas of molecules and to the right of the metal and everywhere in between lies the interface where the gas molecules may lose their chemical identity. H_2 , O_2 ,

H₂O from the right and e from the left arrive at, interact within, and leave the interface at the thermal initial rates, $j_{\text{O}_2} = p_{\text{O}_2}(2\pi m_{\text{O}_2}T)^{-1/2} = 3 \text{ nm}^{-2}\cdot\text{ns}^{-1}$, $j_{\text{H}_2} = p_{\text{H}_2}(2\pi m_{\text{H}_2}T)^{-1/2} = 1\cdot 10^{-1} \text{ nm}^{-2}\cdot\text{ns}^{-1}$, $j_{\text{H}_2\text{O}} = p_{\text{H}_2\text{O}}(2\pi m_{\text{H}_2\text{O}}T)^{-1/2}$, and $j_e = 6\cdot 10^{-1} \text{ nm}^{-2}\cdot\text{fs}^{-1}$. The values of the ratios $j_e : j_{\text{O}_2} : j_{\text{H}_2} : j_{\text{H}_2\text{O}}$ indicate that encounters between the electrons and the molecules within the interface are likely. Electrons e in the bulk of the metal flow in three conduction bands e_6 , h_5 , h_4 . The narrow, anisotropic bands h_4 and h_5 of predominantly 5*d* character stretch from -4.1 to 0.3 eV and from -1.4 to 0.7 eV with respect to the Fermi level, respectively. The remaining fully filled bands of 5*d*-character go down for about -10 eV. The free electron-like, nearly isotropic band e_6 that centers at the Γ point of the Brillouin zone stretches from -1.4 below up to 9 eV above the Fermi level²⁸. In particular, electrons at kinetic energies in excess of 0.7 eV above the Fermi level have to travel in the free electron-like band e_6 . The kinetic energies of the degenerate thermal conduction electrons in the narrow 5*d* bands and in the broad 6*s* bands of Pt are close to their degeneration temperatures of 4.1 eV and 1.4 eV, respectively²⁸. At the electron impact energies comparable to those of the conduction electrons in Pt, the electron scattering experiments against free H₂ and O₂ targets indicate that dissociative electron attachment channels are open²⁸. Therefore, it is hardly surprising that if H₂ and O₂ molecules that adsorb from the gas and electrons that arrive from the metal manage to overlap at the interface, then they may participate in catalytic chemical reactions at the interface on equal footing. The reactions that underlie²⁹ eq. (1) proceed through electron-assisted breakup of molecules into smaller and more reactive fragments, involve the consequent coalescence or further breakup of the fragments, and ultimately end with the desorption of molecules into the gas and the electrons into the metal. In particular, the language of scattering theory is natural here.

Let the gas and the metal (the system) in fig. 1(c) extend arbitrarily far along the normal to the interface. Let the propagation of electrons and molecules deep in the gas and deep in the metal be free, but not within the interface that includes a massive Pt(111) slab. Then the many-body excitations of the system look like the internal and kinetic energy excitations of the free molecules deep in the gas, the internal energy excitations within the interface, and the excitations of the free conduction band electrons deep in the metal. Under these assumptions, the language of the many-body scattering theory with respect to the asymptotic free dynamics of the conduction electrons deep in the metal and that of the free molecules deep in the gas applies.

A remark is called for. If a molecule or an electron leaves the interface into the gas or into the metal, then collisions randomize the initial momentum and energy at a distance of an order of several mean free paths. The fastest channel for energy relaxation of electrons in the high electron density metal Pt is scattering with the electrons and holes near the Fermi level at the length scale set by the inelastic mean free path, whose value GW calculations³⁰ estimate as around 5 nm for electron kinetic energies around the Schottky barrier heights. Since the width of the bulk phonon bands (i.e., the Debye temperature) in Pt(*fcc*) is about 290 K³¹, a temperature comparable to those relevant in this report, phonons are excited throughout the Brillouin zone. In particular, some of these phonons have quasimomenta comparable to those of the electrons, and can significantly alter the propagation directions of the electrons without changing the kinetic energy of the latter. This is to say that elastic scattering increases the length of the paths that electrons have to travel from the interface to the Schottky barrier in the nearly isotropic e_6 band. This report does not discuss these dissipative effects any further. They are certainly important for the interpretation of the experiments, but are nonetheless conceptually secondary to the fast electron mechanism that this report focuses on.

This report adopts the standard nomenclature of many-body scattering theory^{32,33} as follows. Let 1 be any subsystem of the system (fig. 1(c)). Let $\alpha = \{A\}$ be a partition of 1 into bound fragments. The total energy with respect to the center of mass at rest of 1 in an internal energy state $|\overline{\alpha\nu}\rangle$ has a decomposition,

$$E = \chi(\alpha\nu) + t(\alpha\nu p). \quad (7)$$

Here, the internal energy $\chi(\alpha\nu) = \sum_{A\nu \in \alpha\nu} \chi(A\nu)$ is the sum of the internal energies $\chi(A\nu)$ of the individual free fragments A with respect to their centers of mass at rest. The label $\alpha\nu = 0, 1, \dots$ orders the orthonormal states $|\overline{\alpha\nu}\rangle$ according to increasing internal energy. Then, a channel $\alpha\nu$ is the totality $\{|\underline{\alpha\nu p}\rangle\}_p$ of all those wavepackets that differ only by the translational degrees of freedom p of fragments whose internal degrees of freedom reside in the state $|\overline{\alpha\nu}\rangle$. The kinetic energy of the relative translational motion of the centers of mass of the free fragments in α is $t(\alpha\nu p)$. The threshold of the channel $\alpha\nu$ is the lowest possible energy in the channel $\alpha\nu$, i.e., it is the internal energy $\chi(\alpha\nu)$ (since $t(\alpha\nu p) \geq 0$). An arbitrary fully interacting state of 1 admits decomposition into wavepackets of the channels. The S -matrix elements³³ $S(\alpha\nu p \alpha' \nu' p')$, which determine chemical reaction rates, link the free

wavepackets in the past and in the future channels,

$$|\alpha\nu p\rangle = \sum_{\alpha'\nu'p'} S(\alpha\nu p\alpha'\nu'p') |\alpha'\nu'p'\rangle. \quad (8)$$

The S -matrix element connecting different channels in eq. (8) does not vanish only if the total energies in the initial and final channels coincide, and both the channels are open (i.e., the energy exceeds the thresholds for these channels).

The label ν at a given α describes internal degrees of freedom of the free bound fragments, which are exponentially localized. Changes in ν at a given α do not change the topological connectivity of the localized fragments. On the other hand, the label α describes the translational degrees of freedom of the centers of mass of exponentially localized fragments that run away from their common center of mass. It is a change in α that accounts for qualitative changes in the topological connectivity of the exponentially localized fragments upon adsorption-desorption or electron attachment-detachment. Hence, a proper object to deal with here is the eigenblock $E(\alpha)$, which packs all the channels of identical topological connectivity α . The partitions $\{\alpha\}$ of 1 are partially ordered with respect to the domination relation ($\alpha \rightarrow \alpha'$ only if all the fragments in α' belong or coincide with some fragments in α)^{32,33}. This partial order is natural since it classifies independent pathways of breaking up 1 into fragments at costs set by the differences in the break up thresholds. The lowest threshold, $\chi_0(\alpha) = \chi(\alpha 0)$, is a monotone function in α , and $\chi(\alpha\nu)$ is a non-decreasing function of ν within a given eigenblock $E(\alpha)$. Given a stoichiometric composition and a range of the total energies, it is convenient to depict in a graph the relation between those eigenblocks some of whose channels are open in the energy range. The eigenblocks $E(\alpha')$ and $E(\alpha'')$ are adjacent in the graph if $\alpha'_1 \rightarrow \alpha''_1$ for some α'_1 and α''_1 such that $E(\alpha'_1) = E(\alpha')$ and $E(\alpha''_1) = E(\alpha'')$. The lowest threshold $\chi_0(\alpha)$ is then defined on the vertices of the graph and the edges bear labels $\chi_0(\alpha'') - \chi_0(\alpha')$. For example, fig. 3(a) and fig. 4(a) describe the break up of the systems $H_2 + 2e$ and $O_2 + 2e$ into free neutral atoms and electrons.

To account for the geometry of the adsorption system, from now on, let a channel $\alpha\nu$ decompose into the following spatially separated free contributions (fig. 1(c)):

$$\alpha\nu \rightarrow (\alpha\nu)^-; \quad \alpha\nu \rightarrow (\alpha\nu)^0; \quad \alpha\nu \rightarrow (\alpha\nu)^+.$$

Here, $(\alpha\nu)^0$ is a channel that includes a single bound fragment containing the Pt(111) slab as a subfragment (i.e., α^0 is the Pt(111) slab and the electrons and H and O atoms localized

within it). The subchannel $(\alpha\nu)^+$ includes only the H- and O-bound fragments in the gas, the subchannel $(\alpha\nu)^-$ — the electrons in the metal.

A diagram

$$[\alpha\nu \rightarrow \alpha'\nu'] = \begin{array}{ccc} & (\alpha\nu)^+ & (\alpha'\nu')^+ \\ & \downarrow & \uparrow \\ & (\alpha\nu)^0 & \longrightarrow (\alpha'\nu')^0 \\ & | & | \\ e_{(\alpha\nu)^0} & \longrightarrow & e_{(\alpha'\nu')^-} \\ & \uparrow & \downarrow \\ & (\alpha\nu)^- & (\alpha'\nu')^- \end{array}$$

depicts an S -matrix element, which reads as ‘an inbound channel $\alpha\nu$ from $E(\alpha)$ that has components from the gas in $E(\alpha^+)$, from the interface in $E(\alpha^0)$, and from the metal in $E(\alpha^-)$ becomes an outbound channel $\alpha'\nu'$ from $E(\alpha')$ that has components from the gas in $E((\alpha')^+)$, from the interface in $E((\alpha')^0)$, and from the metal in $E((\alpha')^-)$ because of the coupling through the S -matrix.

Diagrams $[\alpha\nu \rightarrow \alpha'\nu']$ are global objects that do not point explicitly to where an event occurs within the interface. However, it is natural to think that diagrams $[\alpha\nu \rightarrow \alpha'\nu']$ must arise from their localization to sites within the interface. Let a set of regions $\{U\}$ (sites) cover the interface appropriately so that the content of a U can be labeled in a chemically meaningful way by any distinguished free channel $(\alpha\nu)_U^0$ that involves the set of the H and O atoms and the electrons within U for a long enough time. A choice of a particular $\{U\}$ rests implicitly on a semiclassical assumption of meaningful uncertainties for simultaneous measurements of the total energy, linear momentum, and a particular H or O atom content during a long enough time compared to the duration of a reactive event within U . If the electrons of the metal scatter independently over U , the S -matrix is determined by a local diagram

$$[\alpha\nu \rightarrow \alpha'\nu']_U = \left[\begin{array}{ccc} & (\alpha\nu)^+ & (\alpha'\nu')^+ \\ & \downarrow & \uparrow \\ & (\alpha\nu)^0 & \longrightarrow (\alpha'\nu')^0 \\ & | & | \\ e_{(\alpha\nu)^0} & \longrightarrow & e_{(\alpha'\nu')^-} \\ & \uparrow & \downarrow \\ & (\alpha\nu)^- & (\alpha'\nu')^- \end{array} \right]_U,$$

which reads as ‘in a small region of the interface U , an initial channel $\alpha\nu$ that looks like free $(\alpha\nu)_U^0$ maps to a final channel $\alpha'\nu'$ that looks like $(\alpha\nu)^+$ propagating into the gas, $(\alpha\nu)^-$

propagating into the metal, and $(\alpha'\nu')^0$ being the excited interface, and these channels are precisely all the channels such that the wavefunction at present concentrates mostly in a neighborhood of U' . Different parts of the inbound and outbound wavefronts are the result of interference of the wavefronts coming to or from local regions $\{U\}$ of the interface so that the S -matrix expresses in terms of local diagrams. Diagrams $[\alpha\nu \rightarrow \alpha'\nu']_{U'}$ and $[\alpha'\nu' \rightarrow \alpha''\nu'']_{U''}$ can be combined into sequences $[\alpha\nu \rightarrow \alpha'\nu']_{U'} \rightarrow [\alpha'\nu' \rightarrow \alpha''\nu'']_{U''}$, ordered by chronological precedence, by joining stoichiometrically compatible left and right ends of diagrams over U' and U'' , which end up over a U . It is then an assumption that the local diagrams and their sequences define the global S -matrix elements. The interaction between the content of U and the interface renormalizes the bound states, thresholds, and resonances, which are associated with the ‘free’ local components of the S -matrix over U . Over a given U , the local diagrams arrange on graphs such as those in fig. 3(b) and fig. 4(b), which are similar to those in fig. 3(a) and fig. 4(a) but also account for the presence of the interface. Let $\chi((\alpha\nu)_U^0)$ be a local ‘threshold’, which is intuitively the minimum energy in U such that $(\alpha\nu)_U^0$ cannot be ignored in $(\alpha\nu)$. The local thresholds labels the arrows in the graph. This reports needs to qualitatively describe those local diagrams that may contribute to fast electron flux in eq. (1).

Among possible channels that may arise in the adsorption system only few can be open at the conditions relevant to this discussion. Let ϵ_U^0 be the internal energy that concentrates in U . The energy ϵ_U^0 assumes values according to a non-equilibrium probability distribution whose qualitative structure needs to be determined. This distribution has a locally equilibrium contribution which depends on the local temperature at mesoscopic time and length scales, which defines an average thermal energy scale ϵ^{\min} . The local temperature depends on the rate of energy exchange with the environment in the actual open physical system through the energy balance equation in a macroscopic steady state. The latter arises from the competition between the heat transport flux away from U and heat sources within U at the interface. The heat sources due to eq. (1) have a power density of $R(\text{H}_2\text{O})\Delta H_{\text{H}_2\text{O}} \lesssim 105 \text{ W/m}^2$, where the reaction rate $R(\text{H}_2\text{O}) \lesssim 50$ molecules per a site of Pt(111) per second at the experimental temperatures and H_2 partial pressures¹. The actual heat transport flux is at least the local equilibrium heat conductivity flux that neglects the heat transfer by a non-equilibrium distribution of electrons, holes, and internally excited molecules. It is straightforward to check along the lines of Refs. 34 that transport limita-

tions due to a finite rate of heat transfer results in an elevation of the surface temperature above the thermodynamic equilibrium value in the range $10^{-6} - 10^{-5}$ K, or equally small value of the internal energy enhancement in these steady states. ϵ^{\min} is on the order of the thermal energy ($k_{\text{B}}T$) or around 0.02 – 0.03 eV per internal degree of freedom. The energy scale ϵ^{\min} restricts types of bound fragments. Only those fragments whose lowest breakup threshold exceeds ϵ^{\min} per fragment are likely to remain bound in the thermal distribution in U . In particular, ϵ^{\min} rules out weakly bound neutrals (e.g., $(\text{H}_2)_{\text{n}}$, $(\text{O}_2)_{\text{n}}$), which are likely only at low temperatures.

The distribution of ϵ_U^0 also includes a microscopic contribution that fluctuates fast at the length scale of U and at the time scale of an individual reactive event. A particular maximum energy scale ϵ_U^{\max} sets the width of this distribution. The channels satisfying $\chi(\alpha\nu)_U \gg \epsilon_U^{\max}$ are likely to remain closed and irrelevant. Changes in the internal energy localized within U on the time scale of an individual chemical event, ϵ_U^{\max} , can be on the order of the thermodynamic reaction heat $\Delta H_{\text{H}_2\text{O}}$ per H_2O in U . Thus, the estimated scale ϵ_U^{\max} limits the channels that may contribute to eq. (8) as follows. All channels that include cations or anions are practically closed. Indeed, the minimum thresholds for electron detachment, anion detachment, and cation detachment into the gas well exceed ϵ_U^{\max} since the electronic workfunctions for the clean or covered Pt surfaces¹¹ exceed 5 eV. Furthermore, no electron emission, anion emission, nor cation emission has been seen from Pt(111) surfaces during H_2 oxidation at the conditions that would permit such observations. The measured heats of adsorption of the neutrals (0.3 – 2.2 eV) and their electron affinities ($\lesssim 2$) and ionization potentials $\gtrsim 10$ eV set the thermodynamic estimates for minimum thresholds for emission of cations and anions into the gas. The values of the adsorption energies, however, do not preclude scattering into those channels that include the neutrals in the gas. It is known that the only bound neutrals that form at the conditions relevant to this report are H_2 , O_2 , and $(\text{H}_2\text{O})_{\text{n}}$. Hence, only the following types of the diagrams are conceivable: (i) $(\alpha\nu)^+ = (\alpha\nu)^- = \emptyset$ (an internal excitation of the interface); (ii) $(\alpha\nu)^+ = \emptyset$ but $(\alpha\nu)^- \neq \emptyset$ (electron attachment or detachment into the metal without molecular adsorption or desorption); (iii) $(\alpha\nu)^+ \neq \emptyset$ but $(\alpha\nu)^- = \emptyset$ and all fragments in $(\alpha\nu)^+$ are neutral (pure molecular adsorption-desorption); (iv) $\alpha^+ \neq \emptyset$ and all fragments in α^+ are neutral, and $\alpha^- \neq \emptyset$ (simultaneous adsorption-desorption and electron attachment-detachment).

Let $\zeta_U(\alpha\nu)$ be the electric charge of $(\alpha\nu)_U^0$ that concentrates in U in the sense that it is

the charge (in the units of the electron charge) of a free channel $(\alpha\nu)_U^0$ as if it were a part of the interface modulo any particle exchange with the environment. Let $\zeta_U(\alpha\nu \rightarrow \alpha'\nu')$ denote the change in the bound charge at the interface along the diagram $[\alpha\nu \rightarrow \alpha'\nu']_U$. Among these conceivable diagrams, the change in the charge $\zeta_U(\alpha\nu \rightarrow \alpha'\nu')$ selects reduction ($\zeta_U(\alpha\nu \rightarrow \alpha'\nu') > 0$), oxidation diagrams ($\zeta_U(\alpha\nu \rightarrow \alpha'\nu') < 0$), and redox diagrams ($\zeta_U(\alpha\nu \rightarrow \alpha'\nu') = 0$). Reduction diagrams lead to negatively charged intermediates, which are strongly bound at the interface at an internal energy ϵ whereas oxidation diagrams lead to intermediates of lower charges or to neutral products at an internal energy $\epsilon' < \epsilon$. Those redox diagrams that can be cut into dual sequences of reduction and oxidation diagrams over a site U define electron pumps over U , which localize metal electrons along the reductive diagrams and delocalize the localized electrons along the oxidative diagrams. In a pump, the terminal channel of a reductive diagram, which is also the initial channel of the consecutive oxidative diagram, often involves several negatively charged interfacial intermediates. If these intermediates must collide for the oxidative diagram to proceed forward, the repulsion barrier must impede the oxidative diagram. However, this barrier can be circumvented by discharging one of the colliding intermediates through electron emission in an auxiliary channel that couples appreciably to the terminal channel of the oxidative diagram. The lowest accessible threshold among the auxiliary channels that circumvents the barrier along a pump compatible with eq. (1) defines the activation barrier, χ^\ddagger . If the total energy of the colliding fragments is $\epsilon \geq \chi^\ddagger$, then up to $\chi^\ddagger - \epsilon'$ can become kinetic energy including that of the detaching translationally excited conduction electrons. Since $\epsilon' < \epsilon < \chi^\ddagger$, the term ‘threshold’ is a bit of a misnomer. The negatively charged intermediates at ϵ' are already in the electron detachment continuum, and should be considered as metastable resonances that destabilize at the energies above χ^\ddagger . However, χ^\ddagger should be related to thresholds for the ‘free’ channels.

The remainder of this report proceeds as follows. First, given a choice of sites $\{U\}$, energetically accessible reduction and oxidation diagrams over U need to be enumerated. Then, these diagrams define various redox pumps, which, in turn, define fast electrons as translationally excited electrons that emerge above the local ‘thresholds’ of the pumps. Fragments that define fast electron mechanisms can be diverse. Given a region U occupied by H and O atoms during a short enough time, nothing so far precludes fragments such as “O₂”, “O₂[−]”, “O[−]”, “H₂”, “H[−]”, “OH”, “OH[−]”, “(H₂O)_n”, “(H₂O)_nO[−]”, “(H₂O)_nOH[−]”, etc., from ap-

pearing in $(\alpha\nu)^0$, and nothing precludes reduction, oxidation, and redox diagrams connecting these channels to contribute to fast electron flux. These fragments and diagrams can be very different chemically. However, they fall under the same heading. The experimental evidence and quantum chemistry calculations further narrow down this picture.

III. MECHANISM OF H_2 OXIDATION ON Pt(111)

A. Events related to oxygen adsorption-desorption

O_2 adsorbs dissociatively on Pt(111) in a broad temperature range 160 – 700 K, and pairs of chemisorbed oxygen atoms, “ $\text{O}^- + \text{O}^-$ ”, associatively desorb at $\gtrsim 700$ K³⁵. The dissociative adsorption is a sequential electron attachment process. O_2 remains physisorbed and uncharged, “ O_2 ”, at $T \lesssim 45$ K^{36–39}, it converts to the charged superoxide, “ O_2^- ”, in the temperature range 90 – 135 K^{40,41}, and then to the charged peroxide, “ O_2^{2-} ”, in the temperature range 135 – 150 K^{36–38}, and then to the pair of oxygen ions, “ $\text{O}^- + \text{O}^-$ ”, at higher temperatures. The observed increase in the electronic workfunction of Pt(111) upon adsorption¹¹, core level spectroscopies^{37,38}, the O–O bond elongation, and electronic structure calculations⁴² all indicate that the negative charge progressively increases from virtually none in “ O_2 ”, to larger values in “ O_2^- ” and in “ O^- ”, due to charge transfer from the metal to interfacial electronic states derived from the lowest unoccupied molecular orbitals (LUMO) of O_2 . The dependence of O_2 sticking probability on the incidence angle and the impact kinetic energy⁴³ points to a sequential dissociative electron attachment-adsorption mechanism. The saturation coverage upon exposure of Pt(111) to O_2 at $T \gtrsim 150$ K is 0.25 monolayer (ML, $1 \text{ ML} = 1.58 \cdot 10^{19} \text{ m}^{-2}$) in a structure that forms domains of a long-range ordered honeycomb $p(2 \times 2)\text{-O}_{\text{fcc}}$ pattern in register with Pt(111) such that every other *fcc* site is vacant⁴⁴. The $p(2 \times 2)$ structure is observed already at coverages lower than the saturation coverage suggesting island formation³⁵ because of the attractive longer-range oxygen-oxygen surface interaction⁴⁵. The internal energy that oxygen-platinum bonds store is negative enough to dissociate O_2 during adsorption and also to release heat; the heat of dissociative adsorption of O_2 on Pt(111) varies approximately linearly with the oxygen coverage from the initial value of -2.2 eV down to -2.0 eV at the saturation coverage. A fraction of the internal energy change upon O_2 adsorption converts into the non-thermal

kinetic energy of the pair of “O⁻” emerging in O₂ dissociation at separations as large as 5.6 Å at 160 K in the low coverage limit⁴⁶.

The above discussion suggests that a minimal model of O₂ adsorption-desorption at a site U is the time evolution in the free system $2\text{O} + 2e$ that attaches to the site U by the interaction. In particular, the local diagrams in figs. 2(a) to 2(c) should play a role in O₂ adsorption on Pt(111). The channels of $2\text{O} + 2e$ system organize on the lattice in fig. 3(a). The nodes of the lattice are the channels, which belong to the products of the eigenblocks $E(\text{O})$, $E(\text{O}^-)$, $E(\text{O}_2)$, $E(\text{O}_2^-)$, and $E(e)$. By definition, the O ground-state multiplet $2p^4\ ^3P$ spans $E(\text{O})$ (a gap of about 2 eV separates this multiplet from the rest of the infinite discrete spectrum of O). The eigenblocks $E(\text{O}^-)$, $E(\text{O}_2^-)$, and $E(\text{O}_2)$ contain finitely many states since their respective lowest break-up thresholds are two-cluster thresholds, and the interactions between the respective breakup fragments, $\text{O} + e$, $\text{O}_2 + e$, $\text{O} + \text{O}$, decay faster than the inverse square distance. The states of the O⁻ ground-state multiplet 2P span $E(\text{O}^-)$, and should exhaust the discrete spectrum of O⁻. The states in $E(\text{O}_2)$ lie below $\chi_0(\text{O} + \text{O})$, and are the ro-vibrational states of the five electronic terms whose adiabatic potentials correlate with the pair of the atomic ground-states in $E(\text{O} + \text{O})$ (fig. 3(b)). The eigenblock $E(\text{O}_2^-)$ includes the ro-vibrational states of the term $(3\sigma_g)^2(1\pi_u)^4(1\pi_g)^3 X^2\Pi_g$ just below $\chi_0(\text{O}_2 + e)$. The adiabatic ground state potential of $X^2\Pi_g\text{O}_2^-$ dissociates to $^2P\text{O}^-$ and ^3PO . It ceases to exist as a real-valued function in the region of the vertical electron autodetachment continuum at bond lengths shorter than $l_c \approx 1.2\text{ Å}$ (such that $\mathcal{E}(^2\Pi_g\text{O}_2^-, l_c) = \mathcal{E}(^3\Sigma_g^-\text{O}_2, l_c)$)^{47,48}. In particular, the electron detachment continuum $\text{O}_2 + e$ at $\epsilon > \chi_0(\text{O}_2)$ features the electron attachment resonances $(1\pi_u)^4(1\pi_g)^3\ ^2\Pi_g$ and $(1\pi_u)^3(1\pi_g)^4\ ^2\Pi_u$, which results in the enhancement of inelastic scattering of slow electrons on O₂ at $v = 0, 1, 2, 3$ due to formation of $X^2\Pi_g$ below $\chi_0(\text{O}_2)$ and then resonances above $\chi_0(\text{O}_2)$. The real part of the $^2\Pi_g$ complex adiabatic potential of O_2^- intersects with the O₂’s $X^3\Sigma_g^-$ adiabatic potentials at $\chi_0(\text{O}_2)$, and $a^1\Delta_g\text{O}_2$ at 1.4 eV, above $\chi_0(\text{O}_2)$ at l shorter than the equilibrium bond lengths of O_2 ⁴⁷.

The interaction between O₂ and the interface shifts the free channels in the energy, lifts the orbital degeneracies, and gives rise to bonding and antibonding bands due to the hybridization of the $2p_{\text{O}}$ and the $5d_{\text{Pt}}$ -orbitals at the interface. Figure 3(b) shows that the eigenblocks shift by the thresholds for desorption so that $E(\text{“O}^-”)$ and $E(\text{“O}_2^-”)$ stabilize significantly with the former having the lowest energy while the neutral eigenblocks $E(\text{“O”})$ and $E(\text{“O}_2”)$ remain nearly unaltered by the weaker physisorption interaction. Figure 7

shows the density of the electronic states at “O”, and indicates how the electron acceptor antibonding π_g LUMO of O_2 splits into π_\perp and π_\parallel components by the interfacial electric field, and then hybridizes with the platinum $5d$ bands at the interface. The bonding and some antibonding states are occupied by the electrons. In the saturation coverage structure, $p(2 \times 2)-O_{\text{fcc}}$ (fig. 9(a)), the excesses of electrons at the $2p_o$ orbitals and the depletion of electrons at the $5d$ orbitals are readily seen within the triangle of the interfacial Pt sites surrounding the fcc hollow sites in the interfacial layer, as well as in the d_{z^2} orbital of the Pt atom just beneath the fcc hollow site. It is further known from the experiment and quantum chemistry calculations based on the complete active space method that the $\pi_{g\parallel}$ - and $\pi_{g\perp}$ -derived states shift, respectively, from 4.8 eV and 4.9/5.9 below the Fermi level in O_2^- , while shifting to 1.6 eV 0.2 in O_2^{2-} ⁴⁹. Further dissociation of O_2^{2-} gives rise to a pair of O^- whose $2p$ states shift down to 6.5 eV below the Fermi level²⁸.

The above picture suggests that fast electrons may arise in oxygen desorption as follows (see fig. 3(b)). Let ϵ_U^0 be the total energy localized around “ $O^- + O^-$ ” above the ground state. If $\epsilon_U^0 \lesssim \chi_0(\text{“}O_2^- \text{”})$, the excitations localize at “ $O^- + O^-$ ” in U . However, if $\chi_0(\text{“}O_2^- \text{”}) < \epsilon_U^0 < \chi(\text{“}O_2^- \text{”}\nu) < \chi_0(\text{“}O_2 \text{”})$ the excitations involve electrons translationally excited in the channels “ O_2^- ” $0, \dots, \text{“}O_2^- \text{”}\nu$ at the kinetic energies $\epsilon_U - \chi(\text{“}O_2^- \text{”}\nu)$. The remaining energy localizes around “ $O_2^- \text{”}\nu$ ” in U . If further $\chi_0(\text{“}O_2 \text{”}) < \epsilon_U^0 < \chi(\text{“}O_2 \text{”}\nu) < \chi_0(O_2)$ the electron detaches into any of additional channels “ O_2 ” $0, \dots, \text{“}O_2 \text{”}\nu$ at the kinetic energies $\epsilon_U - \chi(\text{“}O_2 \text{”}\nu)$ with the remainder being the internal energy of the interface around “ $O_2 \text{”}\nu$ ”. Finally, if $\chi_0(O_2) < \epsilon_U^0 < \chi(O_2\nu)$, channels open up that involve translationally and rovibrationally excited O_2 and the interface excited internally. O_2 adsorption starts in an excited channel $O_2 + \text{Pt}(111)\nu$ which coexists with many open electron attachment channels at that energy, and progresses towards “ $O^- + O^- \text{”}\nu$ ”.

B. Events related to hydrogen adsorption-desorption

H_2 dissociatively adsorbs on a clean or oxygen-precovered $\text{Pt}(111)$ interface. Furthermore, the $\text{Pt}(111)$ interface must be predominantly covered with oxygen since in the reported experiments ?? the partial pressures of H_2 and O_2 are considerably different, $p_{O_2}/p_{H_2} = 127$, while the initial sticking coefficients around the room temperature, $s_{O_2} = 0.1 - 0.2$ and $s_{H_2} = 0.1 - 0.2$, are comparable, and the heat of H_2 adsorption (0.7 – 0.8 eV) is lower than

that of O_2 adsorption. Dissociative H_2 adsorption on most metal surfaces results in a charge transfer from the metal that causes formation of “ H^- ” as the increase in the workfunction upon adsorption indicates (a clean $\text{Pt}(111)$ is a notable exception). The H_2 adsorption is weakly activated with activation energy around 0.07 eV. H_2 adsorption is an exothermic process whose initial heat of adsorption is around -0.7 eV per an H_2 . Preferred hydrogen dissociation sites on the $p(2 \times 2)$ oxygen-covered interface are atop sites furthestmost from the oxygens and, to a lesser degree the bridge sites furthestmost from the oxygen atoms⁵⁰.

Thus, a model of an H_2 adsorption-desorption site U is the free system $2\text{H} + 2e$ that attaches to U through the interaction with the interface. The dissociative electron attachment-detachment and H_2 adsorption-desorption events correspond to the diagrams in figs. 2(d) to 2(g), and the lowest threshold for associative electron detachment and H_2 desorption is around 0.7 eV. Figure 4(a) shows the lattice of channels for $2\text{H} + 2e$. By definition, $\text{E}(\text{H})$ contains only the ground state multiplet $1s^1S$ H (a gap of 10.199 eV, which is well above the relevant energy scale, separates the rest of the infinitely many bound states). The numbers of states in the eigenblocks $\text{E}(\text{H}^-)$ and $\text{E}(\text{H}_2)$ are finite since their lowest breakup thresholds are two-cluster thresholds and the interaction between the respective fragments in the channels $\text{H} + e$ and $\text{H} + \text{H}$ are short-range. The term $1s_{\text{H}}^2 \ ^1S$ spans the eigenblock $\text{E}(\text{H}^-)$. The labels of the states in $\text{E}(\text{H}_2)$ are those of the ro-vibrational states of the electronic term $X^1\Sigma_g$ up to $\chi_0(\text{H}_2)$. Furthermore, since H_2 does not bind an electron ($\chi_0(\text{H}_2) = \chi_0(\text{H}_2^-)$), $\text{E}(\text{H}_2^-) = 0$. However, the continuum spectrum in the channel $\text{H}_2 + e$ exhibits resonances, which are associated with the electronic term $X^2\Sigma_u^+$, and whose adiabatic potential dissociates into $\text{H} + \text{H}^-$. The adiabatic potential of this term is not real, the width of the resonance that determines the imaginary part is about 1 eV⁵¹.

The interaction with the interface stabilizes the anionic eigenblock “ $\text{H}^- + \text{H}^-$ ”, and must also push down the $X^2\Sigma_u^+$ resonances. Along the diagram in fig. 2(d), $\sigma_{\text{H}_2}^*$ and $1s_{\text{H}}$ hybridize with the platinum 5d6s bands at the interface to give rise to the split bonding and antibonding bands. Figure 7 shows the density of the electronic states at “H”. The excess electron density in fig. 9(a) indicates the excess of electrons at the $1s_{\text{H}}$ orbitals of “ H^- ” and the deficit of the electrons at the Pt 5d6s orbitals underneath. Furthermore, the workfunction changes by about -0.1 eV, which is consistent with charge transfer from the interface to H. The bonding $1s_{\text{H}}$ -metal states are 7.3 eV below the Fermi level.

Figure 4(b) describes the general structure of the excitation spectrum that H_2 adsorption-

desorption involves. Let ϵ_U^0 be the energy localized around $H^- + H^-$ in U . If $\epsilon_U^0 < \chi_0(\text{“H}_2\text{”})$, the excitations are localized at the interface around $H^- + H^-$, but if $\chi_0(\text{“H}_2\text{”}) < \epsilon_U^0 < \chi(\text{“H}_2\text{”}\nu) < \chi_0(H_2)$, translationally excited electrons emerge at the kinetic energies $\epsilon_U^0 - \chi(\text{“H}_2\text{”}\nu)$. If furthermore $\chi_0(H_2) < \epsilon_U^0 < \chi(H_2\nu)$ rovibrationally and translationally excited H_2 emerge in the gas. In the H_2 adsorption, an initial channel $(H_2 + \text{Pt}(111))\nu$ couples to electron attachment channels at the same energy.

C. Events related to water formation and adsorption-desorption

1. Direct hydroxyl formation

Two distinct mechanistic regimes underlie eq. (1) and both involve formation of an “OH⁻” or its hydrated forms. If “H₂O” is not present at the interface, the reaction proceeds through recombination of the co-adsorbed “H⁻ + O⁻” into “OH⁻” in an exothermic event at a relatively high activation energy of 0.69 eV⁵².

A minimal model of an adsorption site is the free electron attachment-detachment system $H + O + 2e$ that couples to the adsorption site U by the interaction. Figure 5(a) shows the lattice of channels of $O + H + 2e$. The eigenblocks $E(\text{OH}^-)$ and $E(\text{OH})$ contain finitely many states since the respective lowest breakup thresholds are two-cluster thresholds and the interactions between the fragments $\text{OH} + e$ and $H + O$ are short-range. $E(\text{OH})$ includes ro-vibrational states of the term $X^1\Sigma^+$ for $\chi_0(\text{OH}^-) \leq \epsilon < \chi_0(\text{OH})$. $E(\text{OH})$ encloses the ro-vibrational states of the term $X^2\Pi$ for $\chi_0(\text{OH}) \leq \epsilon < \chi_0(O + H)$.

As fig. 5(b) indicates, the interaction with the interface significantly stabilizes the channels “O⁻ + H⁻”, while leaving it above “OH⁻ + e”. Let ϵ_U^0 be an energy near “OH⁻” in U at the interface. The excitations in the energy range $\epsilon_U^0 < \chi_0(\text{“O}^- + \text{H}^-”)$ are bound, and are localized around “OH⁻” ν at the interface. The channels “OH⁻ + e” ν are open in this energy range of ϵ_U^0 . Furthermore, “O⁻ + H⁻” ν are open at $\epsilon_U > \chi_0(\text{“O}^- + \text{H}^-”\nu)$. If “O⁻0” and “H⁻0” were decoupled, each would be indefinitely stable. However, the coupling between “O⁻” and “H⁻” renders these states metastable towards decay into the true ground state, “OH⁻” and an electron. The repulsion between “O⁻” and “H⁻” creates a barrier, which must suppress the direct diagrams in fig. 2(h). However, a superposition of the diagrams in figs. 2(i) and 2(j) circumvents the barrier, and the minimum threshold for

“O⁻ + H + e” plays a role of the activation barrier. When $\epsilon_U^0 > \chi_0(\text{“O}^- + \text{H} + \text{e”})$, the diagram in fig. 2(h) are likely. The energy ϵ_U^0 may flow into any of the channels “OH⁻ + e” ν with $\chi(\text{“OH}^- + \text{e”}\nu) < \epsilon_U^0$. Assuming $\chi_0(\text{“O}^- + \text{H} + \text{e”})$ is the experimental activation energy, the total energy drop from the activation barrier in the channels “OH⁻ + e” is at least $\chi_0(\text{“H} + \text{O}^- + \text{e”}) - \chi_0(\text{“OH}^- + \text{e”}) = 1.2$ eV. The highest possible kinetic energy of a detaching electron around $\epsilon_U^0 - \chi(\text{“OH}^- + \text{e”}\nu)$ of 1.2 eV may arise in the channel at $\nu = 0$ and the lowest kinetic energy of the electron arises in the channel with the highest ν .

Transition state theory calculations (see the Appendix) on the ground state adiabatic potential surface corroborates this picture. As figs. 9(a,b) show, the co-adsorbed “O⁻” and “H⁻” must overcome an activation barrier, $\chi_{\text{OH(I)}}^\neq = 0.79$ eV, during the up-hill step P'_2 , before “OH⁻” forms during the down-hill step P''_2 . As fig. 8(a) indicates, the excess electron density in fig. 9(a) transforms from the initial $1s_{\text{H}}$ - and $2p_{\text{O}}$ -like distribution to a bond-centered distribution during $P''_{\text{OH(I)}}$, a fraction of the electrons redistributes to the non-bonding $1\pi_{\text{OH}}$, where they remain, while the rest return to the metal. The latter is indicated by the drop in the workfunction in fig. 9(c) and by the increase in the delocalization entropy (see eq. (9)) in fig. 9(d). With the charge now concentrated at the non-bonding lone pairs $1\pi_{\text{OH}}$, “OH⁻” assumes the O-end down position (fig. 9(a)). δs in fig. 9(d) indicates charge transfer from the metal to the interface during P'_2 ; δs then rises rapidly during the down-hill step P''_2 . Hence, electrons flow from the metal to the interface during P'_2 , and then return to the vacant states in the metal conduction band during P''_2 . The energy that these electrons may take is estimated by the energy drop, $\delta u_{\text{OH(I)}} = 1.1$ eV, during P''_2 .

2. *Direct hydroxyl hydrogenation*

When another “H⁻” appears next to “OH⁻”, a water molecule may form. A model of an adsorption site U is the free system $2\text{H} + \text{O} + 3\text{e}$ whose lattice of channels fig. 6(a) shows. The eigenblock $\text{E}(\text{H}_2\text{O})$ contains a finite sequence of ro-vibrational levels of the term $(1b_2)(3a_1)^2(1b_1)^2(4a_1)^0\ ^1A$. Since an electron does not bind to the ground state of an H_2O ($\chi_0(\text{H}_2\text{O}) = \chi_0(\text{H}_2\text{O}^-)$), it has to be that $\text{E}(\text{H}_2\text{O}^-) = 0$. However, the continuum of the system $\text{H}_2\text{O} + \text{e}$ includes electron attachment resonances, $1^2B_1(1b_1 \rightarrow 4a_1)$ at around 6.5 eV $2^2B_1\ 1b_1 \rightarrow 4a_1$ at around 8.5 eV, and $2^2B_2\ 1b_2 \rightarrow 4a_1$ at around 11.8 eV⁵³.

Figure 6(b) is a part of the lattice of channels for $\text{H}_2\text{O} + 3\text{e}$ on Pt(111). The channel

“ $\text{H}_2\text{O} + 3\text{e}^-$ ” is the lowest in energy, which the channels “ $\text{OH}^- + \text{H}^- + \text{e}^-$ ”, “ $\text{O}^- + \text{H}^- + \text{H}^-$ ”, “ $\text{O}^- + \text{H}_2 + 2\text{e}^-$ ”, “ $\text{OH}^- + \text{H} + 2\text{e}^-$ ” follow. Either an isolated “ OH^- ” or “ H^- ” is a bound state in U . However, when “ H^- ” and “ OH^- ” are nearby in U , the lowest energy channel is “ $\text{H}_2\text{O} + 2\text{e}^-$ ”, and the false ground state “ $\text{OH}^- + \text{H}^-$ ” becomes metastable. Nevertheless, the repulsion barrier between the two anions suppresses the direct diagram in fig. 2(l). A diagram [“ $\text{OH}^- + \text{H}^-$ ” \rightarrow “ $\text{OH}^- + \text{H} + \text{e}^-$ ” \rightarrow “ $\text{H}_2\text{O} + 2\text{e}^-$ ”] avoids the barrier, and the lowest threshold for the channel “ $\text{OH}^- + \text{H} + \text{e}^-$ ” serves as the activation barrier in fig. 2(l).

Transition state theory calculations on the ground state adiabatic potential corroborate the latter picture. As fig. 9(a) shows, “ H^- ” from an *fcc* hollow site migrates to a bridge site adjacent to the atop “ OH^- ” during P_4'' , and then moves towards the “ OH^- ” along the asymmetric stretch of the nascent water molecule during P_4' . The energy in fig. 9(b) increases towards the activation barrier, $\chi_{\text{H}_2\text{O}}^\neq = 0.3$ eV, at H_2O^\neq during P_4' . It drops by $\delta u_{\text{H}_2\text{O}}^\neq$ (about 1.2 eV) to the minimum at “ H_2O ” during P_4'' . Meanwhile, the workfunction in fig. 9(c) drops by -0.3 eV during P_4' , and then drops by -0.7 eV during P_4'' , indicating charge transfer to the metal. The transport contribution to the entropy due to the electron emitted into the vacant conduction band in fig. 9(d) stays nearly constant during P_4' but rapidly increases during P_4'' . This behavior is caused by the emptying of the continuum of the $\text{H} \cdots \text{OH}$ LUMO ($4a_1$)-derived states that host the excess charge before the transition configuration, H_2O^\neq as fig. 8(b) illustrates. In other words, H_2O^\neq is an “ $\text{H} \cdots \text{OH}^-$ ” that is just about to desorb while simultaneously autoionizing into the metal conduction band. The energy of about 1.2 eV may flow to the channels (“ $\text{H}_2\text{O} + \text{e}^-$ ” ν) with $\nu = 0$ giving rise to electrons with the highest kinetic energy.

3. *Disproportionation mechanism*

If “ H_2O ” is already within the interface, the disproportionation diagram in fig. 2(k) is open at the activation energy of about 0.13 eV^{54,55}, and is the primary source of the interfacial hydroxyl^{54,56}. The transition state theory calculations corroborate this mechanism. Within the $p(4 \times 2) - 2\text{O}_{\text{fcc}} - 2\text{H}_2\text{O}$ pattern in fig. 10, the “ O^- ” moves from the *fcc* site along a line passing through a bridge site while a hydrogen in the atop “ H_2O ” moves towards the “ O^- ” along the line connecting the atop site and the bridge site facing it. The computed value of the activation barrier is 0.33 eV. The computed energy drop in fig. 10(a) from (TS) to (F)

is 0.67 eV. Meanwhile, the workfunction in fig. 10(b) drops by 0.25 eV from (I) to (TS) and increases by 0.35 from (TS) to (F) as the electrons flow to the $1\pi_{\text{OH}}$ of the nascent “OH⁻” (fig. 10(c)).

4. *Another mechanism of hydroxyl hydrogenation*

An “(H₂O)OH⁻” further recombines with a “H⁻” (fig. 2(l)) at an activation energy lower than that for “OH⁻” formation^{54,55,57}. As fig. 11 shows, a pair of hydrogen-bonded “OH⁻” reside at the bridge sites near an “H₂O”. A hydrogen molecule dissociates nearby at an atop site giving rise to a pair of “H⁻”. As “H⁻” moves towards the “(H₂O)OH⁻”, the transition complex “HO... (HOH₂)” forms such that “H₃O” is a trigonal pyramid with the O – H bonds all of similar lengths. This geometry is reminiscent of a free H₃O⁺, which is unstable in neutral or anionic forms. Therefore, the high energy complex “(OH)(H₃O)⁻” regroups into a pair of “H₂O” and an electron while releasing about 1.7 eV per event. The activation barrier is about 0.3 eV. The workfunction in fig. 11(b) increases towards the transition configuration from (I) to (TS), and then drops from (TS) to (F) as the electrons are returned back to the metal. The delocalization entropy in fig. 11(c) also increases past (TS), which is consistent with the release of the electrons to the conduction band from (TS) to (F). The structure of the transition state suggests that the activation barrier is the lowest threshold for the channel “(H₃O)(OH)⁻ + e” that circumvents the repulsion barrier in the direct diagram fig. 2(l) along the diagram [“(H₂O)(OH)⁻ + H⁻” → “(H₃O)(OH)⁻ + e” → “(H₂O)₂ + 2e”], which requires that $\epsilon_U^0 > \chi_0(\text{“(H}_3\text{O)(OH)}^- + \text{e”})$. The kinetic energy of the departing electron can be as high as $\epsilon_U^0 - \chi_0(\text{“(H}_2\text{O)}_2 + 2\text{e”})$, which is 1.7 eV for $\epsilon_U^0 = \chi_0(\text{“(H}_3\text{O)(OH)}^- + \text{e”})$.

IV. CONCLUDING REMARKS

This report describes qualitative aspects of a mechanism of electronic excitations, which likely contributes to a flux of fast electrons during catalytic hydrogen oxidation on Pt(111). Translational excitation of the electrons in the metal during eq. (1) arise as a result of surface chemical events that serve as an electron pump. The building blocks that define the pump are pairs of consequent reduction and oxidation diagrams. Delocalized conduction electrons localize at the interface along the reductive leg and then return to the metal during the

oxidative leg of the pump. This picture is reminiscent to that seen in the context of CO oxidation on Pt(111)²⁶.

The reduction diagrams and oxidation diagrams in fig. 2(a) to 2(m) do not necessarily exhaust all types of oxidation and reduction diagrams that may contribute to fast electron production in eq. (1), but these diagrams exemplify a general principle. Intermediates in a Langmuir-Hinshelwood mechanism²⁹ over a metal surface are more often than not negatively charged and their direct recombination is hindered by their mutual repulsion. The barrier is overcome at an energy ϵ_U^0 higher than the lowest threshold $\chi^\#$ for a low-lying electron detachment channel that connects to both the products and the reactants. Such a channel plays a role like that of the transition state. If $\epsilon_U^0 \ll \chi^\#$, the individual negatively charged reactants or products reside in their metastable ground state which may exist for a very long time. However, if $\epsilon_U^0 \gtrsim \chi^\#$, the products and reactants are no longer independent. This mechanism is an intrinsic signature of transitions between localized and delocalized states of molecular electrons, and is different from the electron-hole pair excitation mechanism, which characterizes the response of the interacting and delocalized electrons in a metal to a localized perturbation without internal degrees of freedom. As such, this mechanism is as generic to catalytic chemical reactions as it is to the redox nature of catalysis at metal surfaces.

A quantitative picture of the fast electron mechanism falls beyond the intended scope of this report. Nonetheless a qualitative argument can be made as follows. The interaction that couples the channels is due to the dynamically screened electric field in the metal and the molecular electric field that act together upon a detaching electron. A decaying negative charge distribution creates the screening charge below it. This screening charge is not instantaneous, and the screening field lags behind the source field at the frequency scale of an order of the plasma frequency, which is about 6 eV in Pt. The energy ϵ of 1 – 1.2 above the ground state of “OH⁻ + e” or “H₂O + e” is not small compared to the response time of the metal. The Lorentz force due to this screening electric field and the molecular electric field transfers the momentum to the detaching electrons. This energy transfer mechanism should enhance the scattering into the channels “OH⁻ + e” ν and “H₂O + e” ν at low ν where the electron kinetic energy ($\epsilon_U^0 - \chi(\alpha\nu)$) can be large.

The structure of the deformations of the mass and charge distribution, which leads to change in the number of localized electrons within the interface is obvious already in the

structure of the ground state adiabatic potential. Atoms in molecules undergoing a photochemical reaction may move, semiclassically, under a force whose potential is an excited adiabatic potential. The most likely reaction pathways for the relaxation of the energy of the products are those that bring the configurations of reacting molecules near conical intersections between the ground and excited state adiabatic potentials, i.e., the surfaces in the configuration space where the adiabatic potentials coincide. If the energy flow at conical intersections controls the kinetics of photochemical reactions, the kinetics underlying eq. (1), a chemical reaction at a metal surface, is controlled, by the energy and charge flow over vertical electron detachment threshold surfaces in the configuration space which parameterize those deformations of the configurations of the interfacial species that cause the localized charge carried by the adiabatic ground state to jump.

V. APPENDIX

A. Numerical density functional model

The workfunction change, $\delta\chi = \int x\delta\rho dz$, estimates the adiabatic change in a part of the charge distribution that localizes at the interface. Meanwhile, the entropy change

$$\delta s = k \ln \frac{\Gamma_{\text{bulk}}}{\Gamma_{\text{surf.}}} \quad (9)$$

due to electron delocalization into conduction band quantifies the likelihood of the charge localized at the interface to flow into the vacant delocalized states of the conduction band. Here, Γ_{bulk} and $\Gamma_{\text{surf.}}$ are the number of the vacant electronic states in the conduction band of the bulk metal, and the number of the localized interfacial states, respectively. The second law of thermodynamics requires that $\delta s > 0$ for a spontaneous process, which corresponds to delocalization of the electrons into the conduction band. Here, the statistical weights are determined by the numbers of Kohn-Sham electronic states in a 2 eV window above the Fermi level, which are localized at the active interface ($\Gamma_{\text{surf.}}$) or are within the metal conduction band (Γ_{bulk}), respectively.

Density functional theory calculations with periodic boundary conditions in this work have been done using the Quantum-ESPRESSO suite of computer programs⁵⁸. The exchange-correlation energy is given by the PW91 generalized gradient approximation⁵⁹. The core electrons in H, O [H], Pt[Xe] are described by ultrasoft pseudopotentials, which

are fitted to reproduce the numerical Kohn-Sham orbitals of the atoms⁵⁸. The ultrasoft pseudopotential for Pt includes the scalar relativistic effects as well as the non-linear core corrections. The Kohn-Sham orbitals and the charge density of the valence electrons are expanded into the Fourier series over plane waves with kinetic energies below 612.26 eV and 6122.6 eV, respectively.

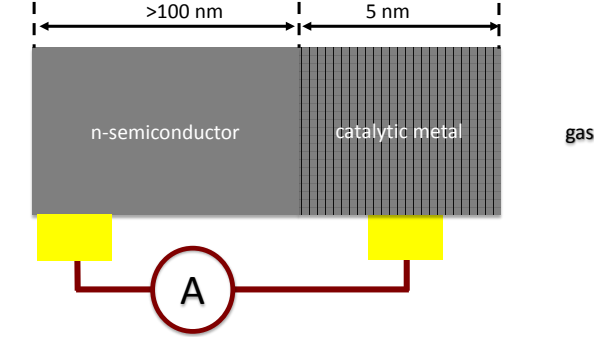
The Pt(111) metal-vacuum interface is modeled by 4 layer hexagonal $p(2n \times 2m)$ -Pt slabs with $n, m = 1, 2$ with a single side open for adsorption. The spacing between the periodically replicated parallel slabs in the direction perpendicular to the surface is maintained above 17 Å to diminish the spurious dipole-dipole interaction between the slabs that asymptotically decreases as the inverse cube of the separation distance. The equilibrium geometries are computed by variable cell relaxation runs until the total force and the stress falls below 0.026 eV/Å and 1 kbar, respectively.

Minimum energy pathways connecting the equilibrium structures on the adiabatic ground state surface are sampled by the nudged elastic bands (NEB) method⁶⁰. A string of intermediate structures interpolating between the initial and final equilibrium structures is varied until forces perpendicular to the path are below 0.094 eV/Å.

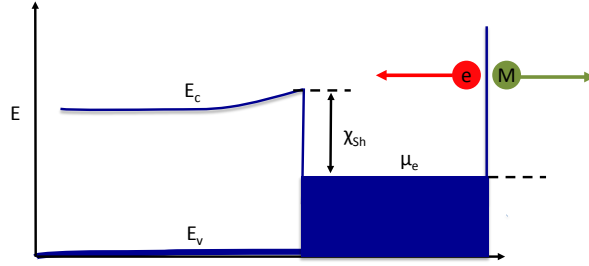
In the NEB and geometry optimization calculations, the integrals over the irreducible surface Brillouin zone of the hexagonal $p(2n \times 2m)$ lattice are discretized over $4/n \times 4/m$ Monkhorst-Pack grid⁶¹ with the Methfessel-Paxton first-order smearing⁶² of 0.204 eV. The reciprocal space integrals in the expressions for the density of electronic states, the electron number density, and the Fermi level are computed over finer $32/n \times 32/n$ Monkhorst-Packs grid using the tetrahedron method⁶³.

ACKNOWLEDGMENTS

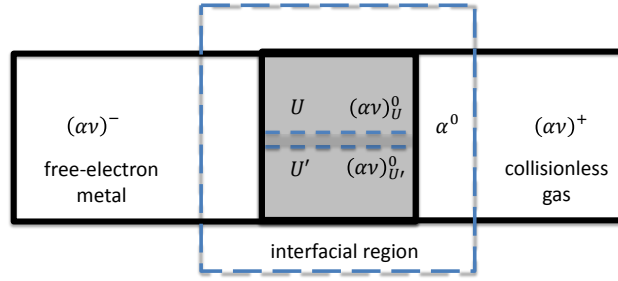
The authors thank L.R. Backer, Y. Borodko, A. Hervier, J.R. Renzas G.A. Somorjai, J.Y. Park for comprehensive and stimulating discussions on the subject of their experimental work. This work was supported by the U.S. Department of Energy, Office of Basic Energy Sciences, Chemical Sciences, Geosciences, and Biosciences Division, through Contract No. DEAC02-05CH11231.



(a)



(b)



(c)

FIG. 1. (a) The Schottky diode. The chemistry takes place at the interface of the gas and the catalytic metal (right), the catalytic metal joins the n -semiconductor over the Schottky contact. The Ohmic contacts (the yellow bars) collect the charge from the catalytic metal and the semiconductor. The wires (brown lines) close the circuit through the ammeter. (b) An energy diagram of the Schottky diode. The chemical potential of the electrons (μ_e) is below the Schottky barrier (χ_{sh}). If a chemical process excites a charge whose kinetic energy at the Schottky contact exceeds the Schottky barrier, the charge enters the semiconductor where it travels in the conduction band (E_c) above the valence band (E_v). The workfunction and the absorption barriers (the rightmost blue vertical line) prevent the electrons from spilling into the gas and the molecular species from entering the metal, respectively. (c) The partition of the space into the metal, the gas, and the interfacial region.

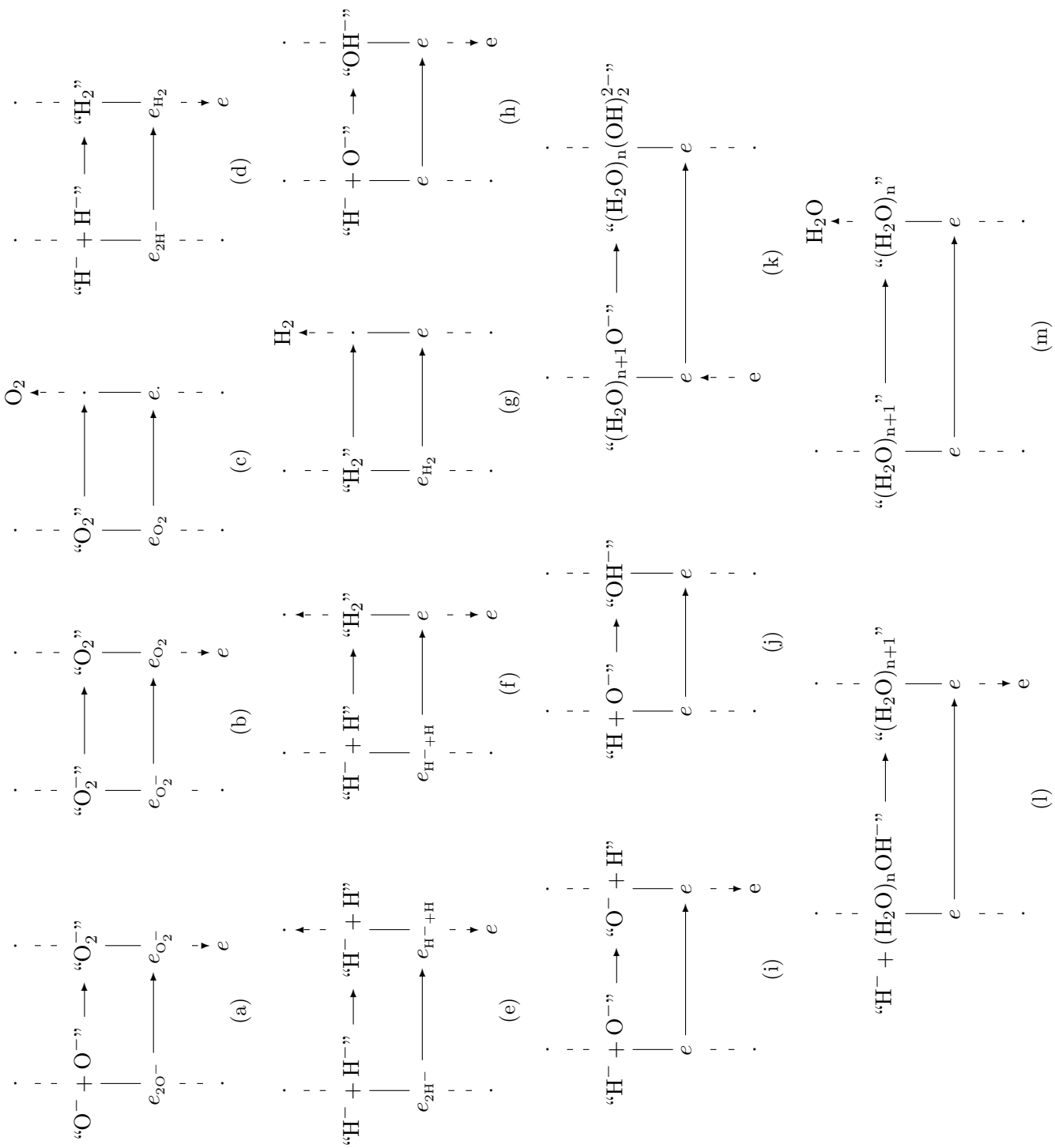


FIG. 2. Some types of local diagrams that contribute to eq. (1).

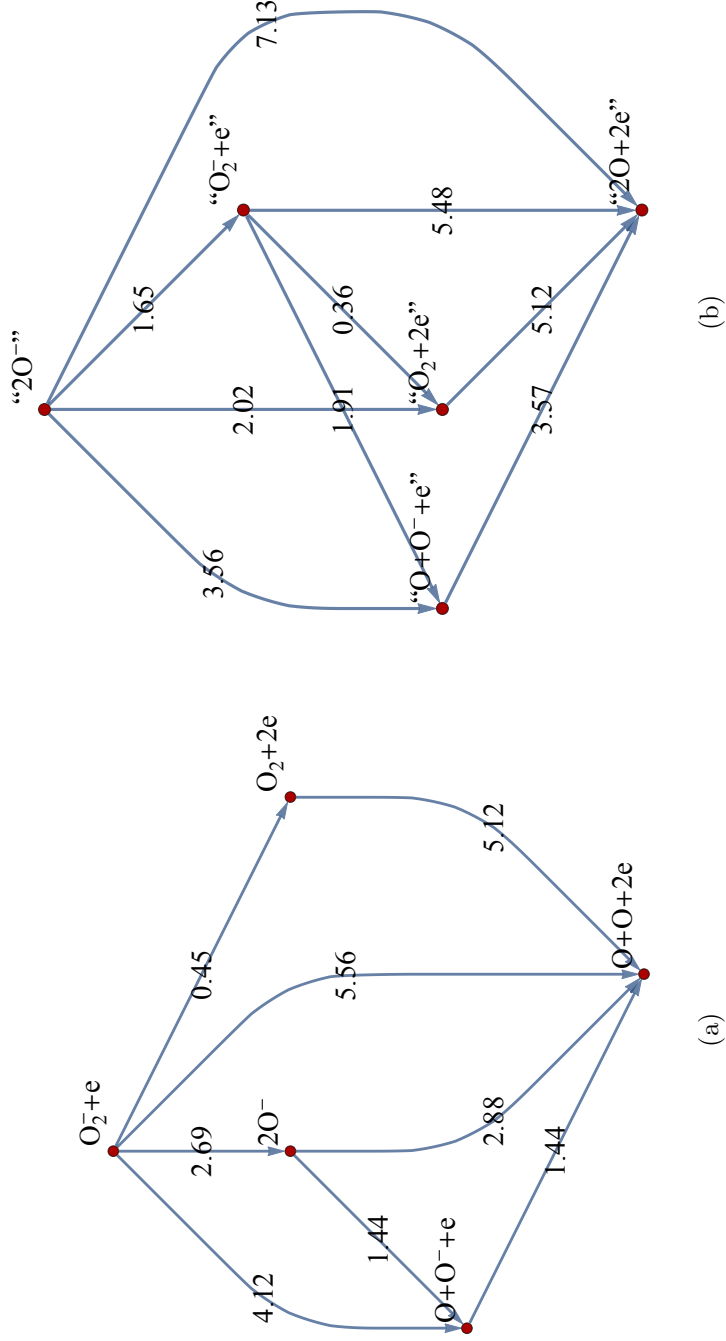


FIG. 3. (a) The lattice of non-equivalent channels for the system $2O + 2e$. The vertices of the lattices are the eigenblocks $E(\alpha)$. (b) The same lattice of the non-equivalent channels after the energy shift due to the interaction (as deduced from the values of the empirical desorption energies). The arrow labels in (a) and (b) are the differences between the experimental values^{13,28} of lowest thresholds for the terminal and initial eigenblocks (in eV).

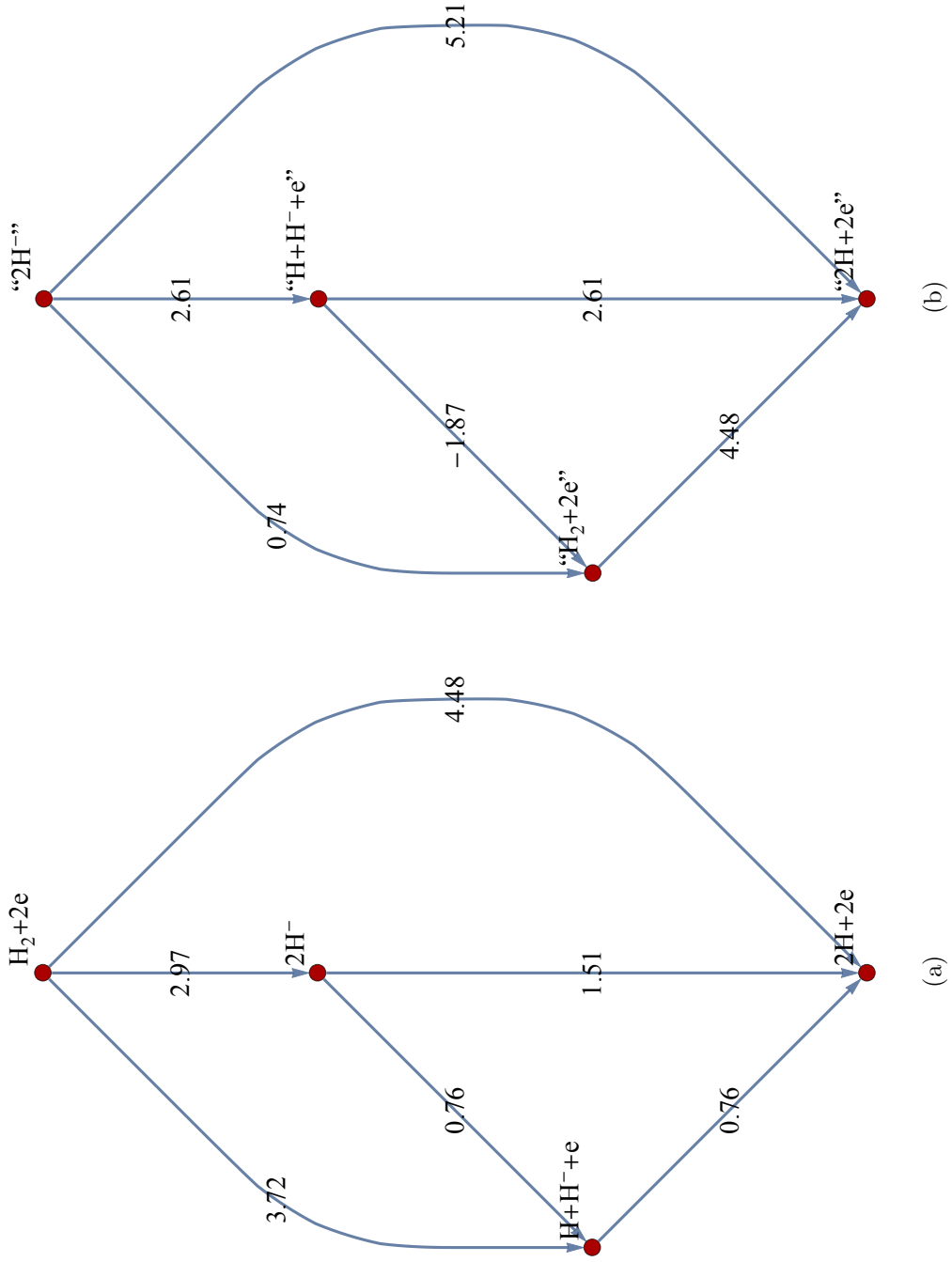
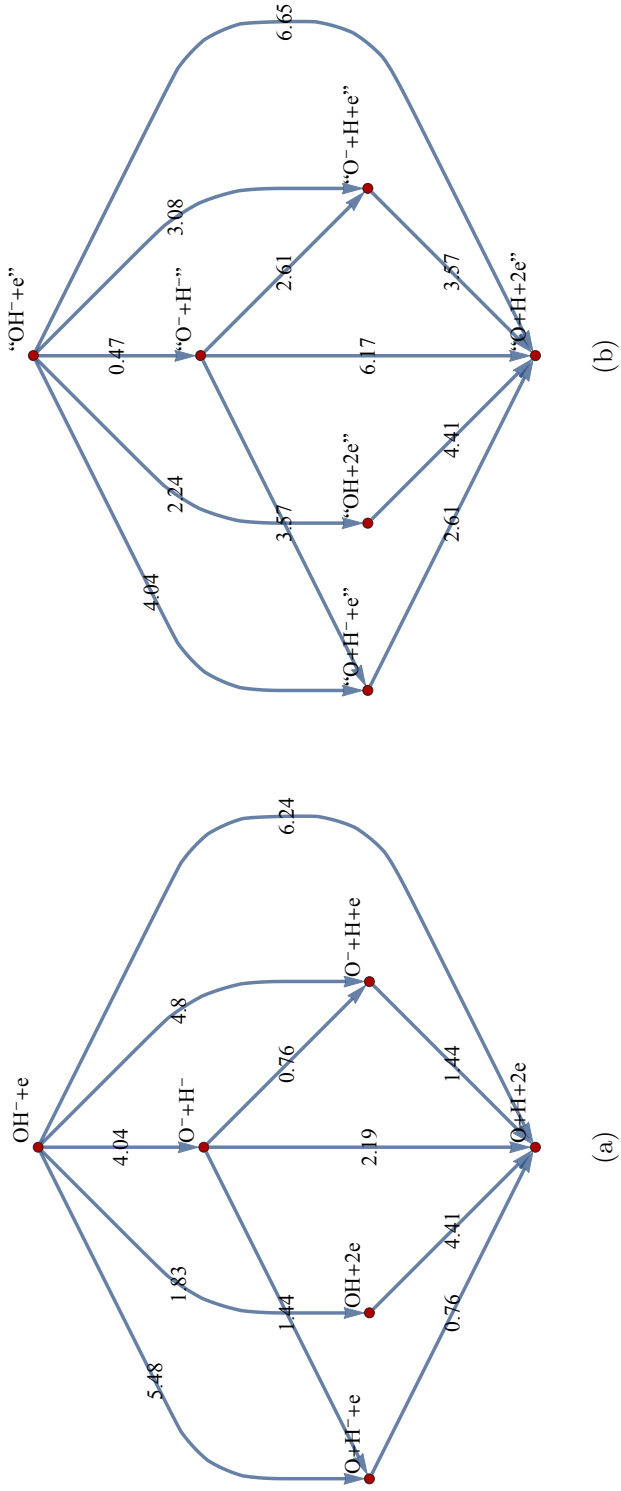


FIG. 4. (a) The lattice of non-equivalent channels for $2H + 2e$. (b) The same lattice of the non-equivalent channels after the energy shift due to the interaction. The arrow labels in (a) and (b) are the differences between the experimental values^{13,28} of lowest thresholds for the terminal and initial eigenblocks (in eV).



(a)

(b)

FIG. 5. (a) The lattice of non-equivalent channels for $H + O + 2e$. (b) The same lattice of the non-equivalent channels after the energy shift due to the interaction. The arrow labels in (a) and (b) are the differences between the experimental values^{13,28} of lowest thresholds for the terminal and initial eigenblocks (in eV).

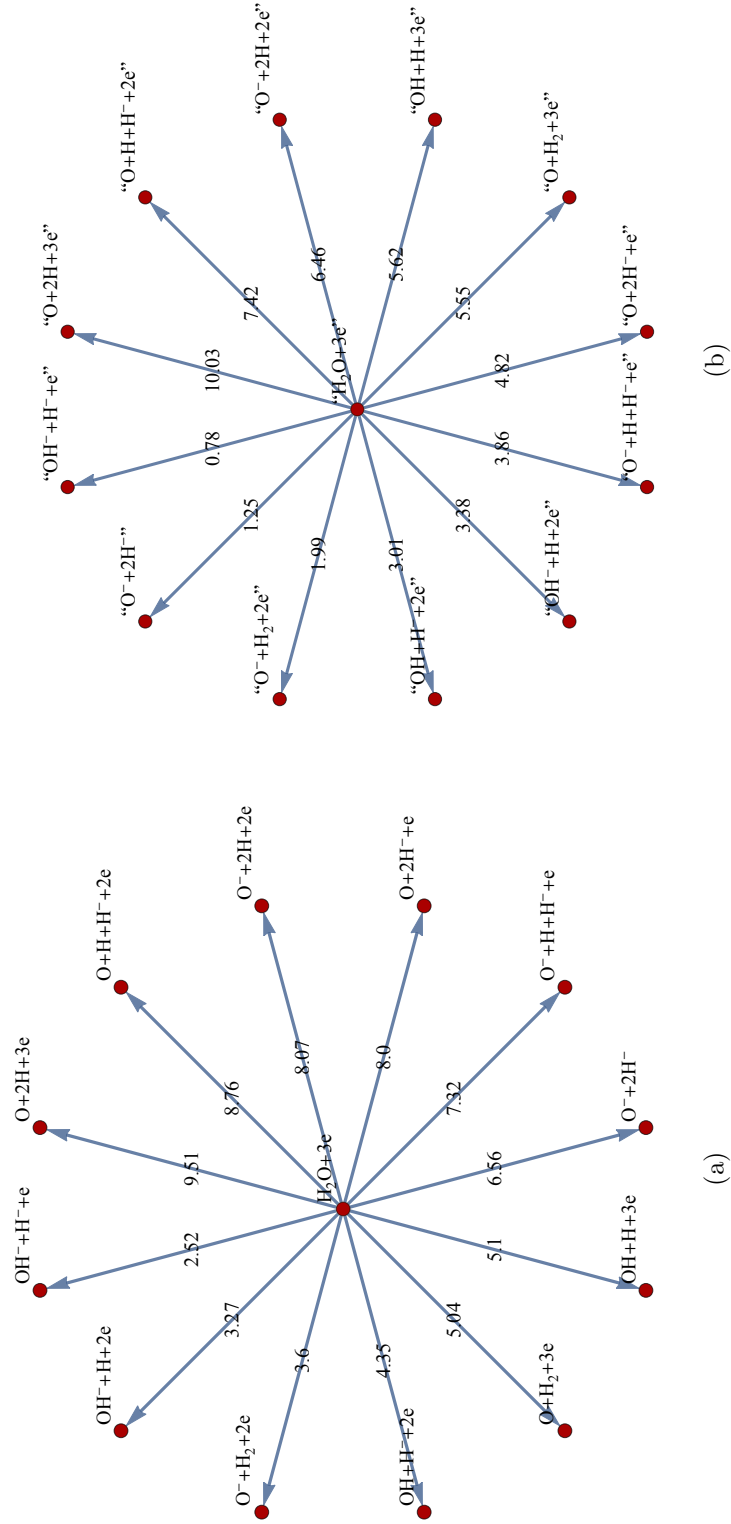


FIG. 6. (a) The channels for $2\text{H} + \text{O} + 3\text{e}$. (b) The channels for $2\text{H} + \text{O} + 3\text{e}$. The arrow labels in (a) and (b) are the differences between the experimental values^{13,28} of lowest thresholds for the terminal and initial eigenblocks (in eV).

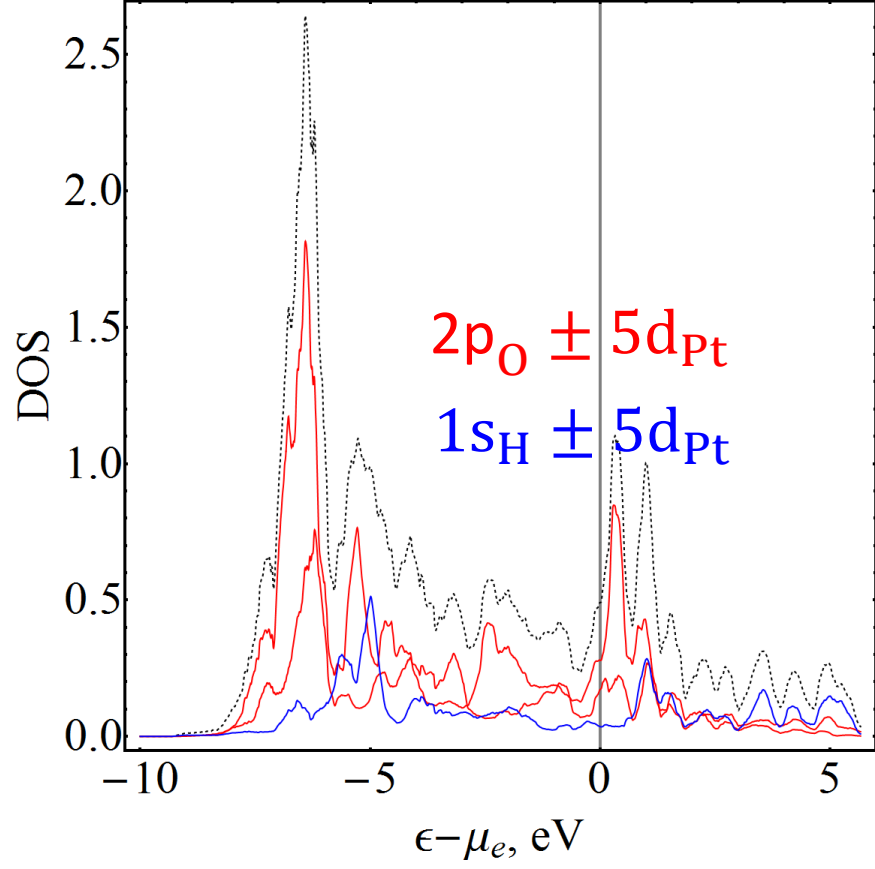


FIG. 7. The density of the Kohn-Sham electronic states at the coadsorbed O and H ions (the black curve), that of the $2p_{O\parallel} \pm 5d_{Pt}$ states (the upper red curves), the $2p_{O\perp} \pm 5d_{Pt}$ states (the upper red curves), that of the $1s_H \pm 5d_{Pt}$ states (the blue curve).

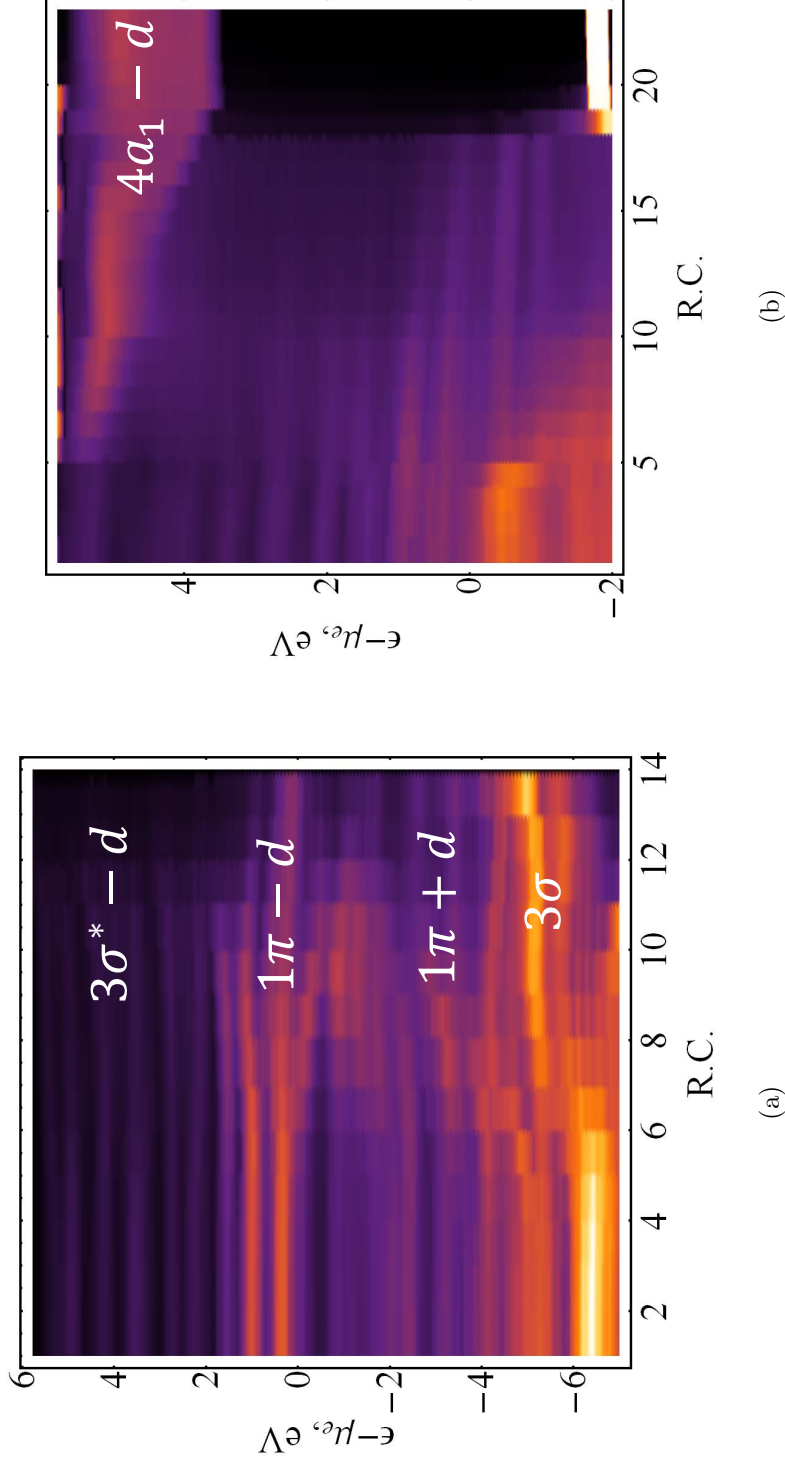


FIG. 8. The density of the Kohn-Sham electronic states along (a) the segment of the reaction path describing the event “ $\text{O}^- + \text{H}^- \rightarrow \text{OH}^- + \text{e}^-$ ”, and (b) along the segment P_4 of the reaction path describing the event “ $\text{OH}^- + \text{H}^- \rightarrow \text{H}_2\text{O} + 2\text{e}^-$ ”. The vertical axis is the Kohn-Sham binding energy with respect to the Fermi level. The horizontal axis is the reaction coordinate. The brighter and darker colors correspond to higher and lower values of the density of states, respectively. In (a), σ_{OH} and σ_{OH}^* and $1\pi_{\text{OH}}$ hybridize with the platinum 5d6s bands at the interface to give rise to the split bonding and antibonding bands. In (b), the $4a_1 - d$ -derived unoccupied states can take late in the reaction the electrons that previously reside within the occupied states.

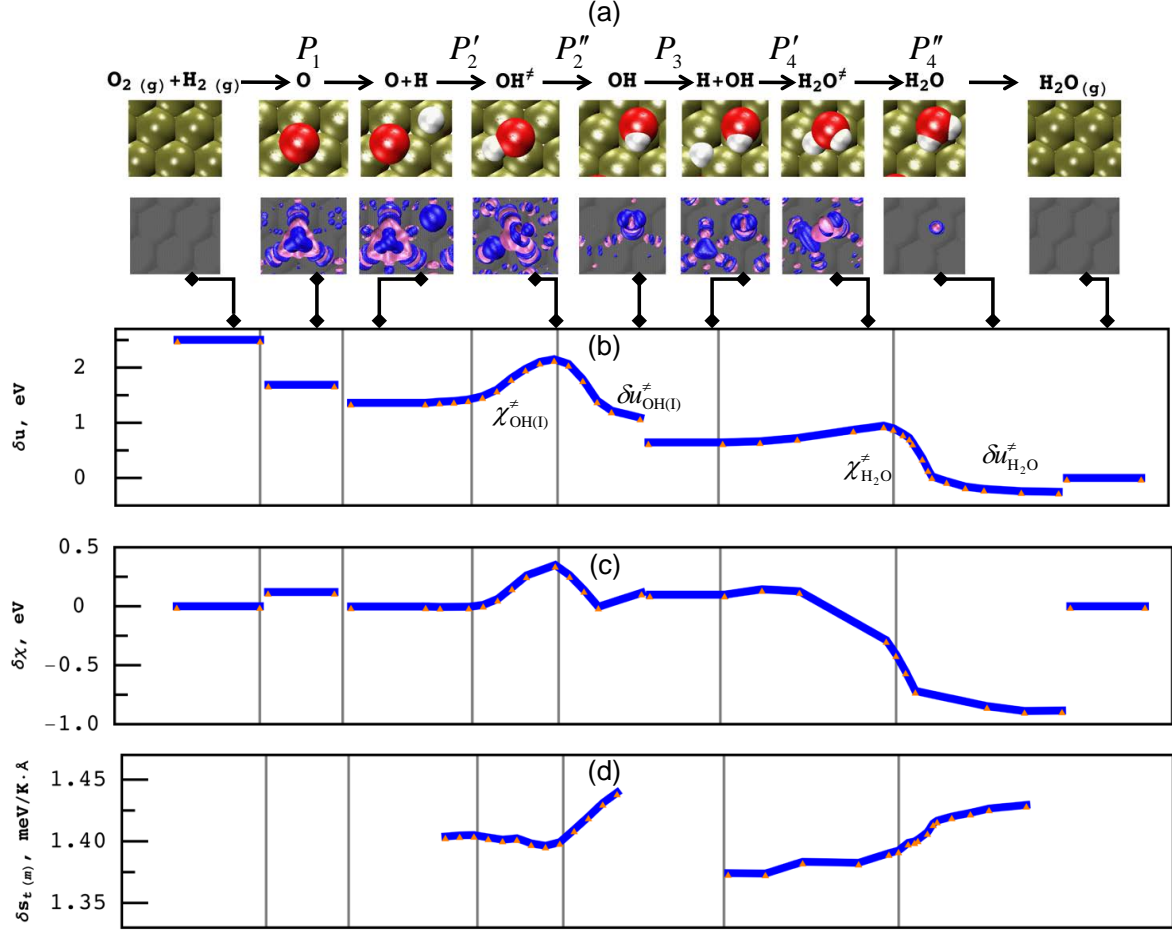


FIG. 9. Along minimum energy reaction paths are shown: (a) the surface oxygen (red balls) and hydrogen (white balls) atoms on Pt(111) (upper row), and the surface electron density ± 0.005 contour values relative to that decoupled from the metal adsorbate layer and that of Pt(111) (blue and pink represent build up and depletion of electrons, respectively); (b) the changes in the energy with respect to the clean Pt(111) slab and a free H_2O ; (c) the workfunction relative to clean Pt(111) slab; (d) the entropy gain upon transferring the electrons from the electronic states localized at the active interface to the metal conduction band (see the appendix).

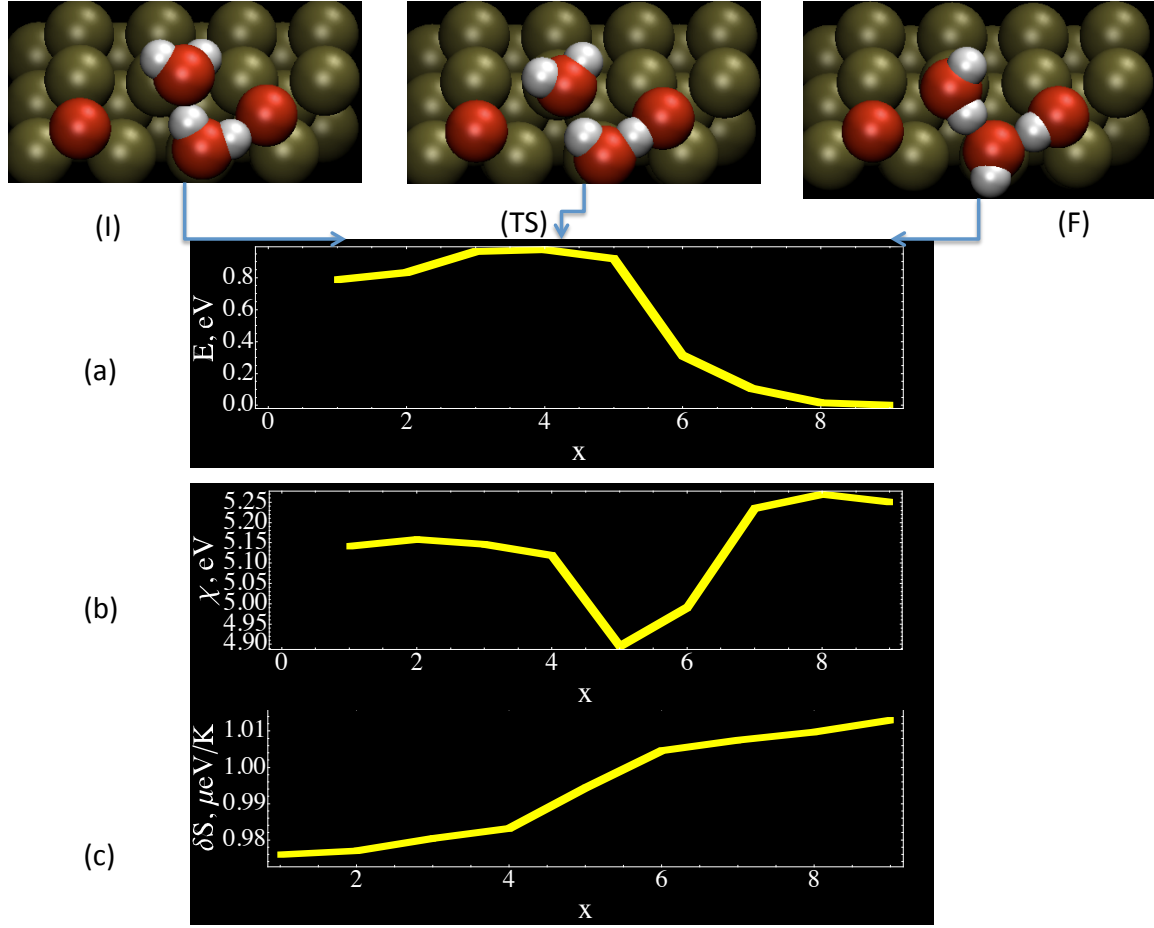


FIG. 10. The change in the energy (a), the workfunction (b), and the electronic delocalization entropy (c) along a minimum reaction path connecting the initial state (I) through the transition state (TS) to the final state (F) for the pathway eq. (5).

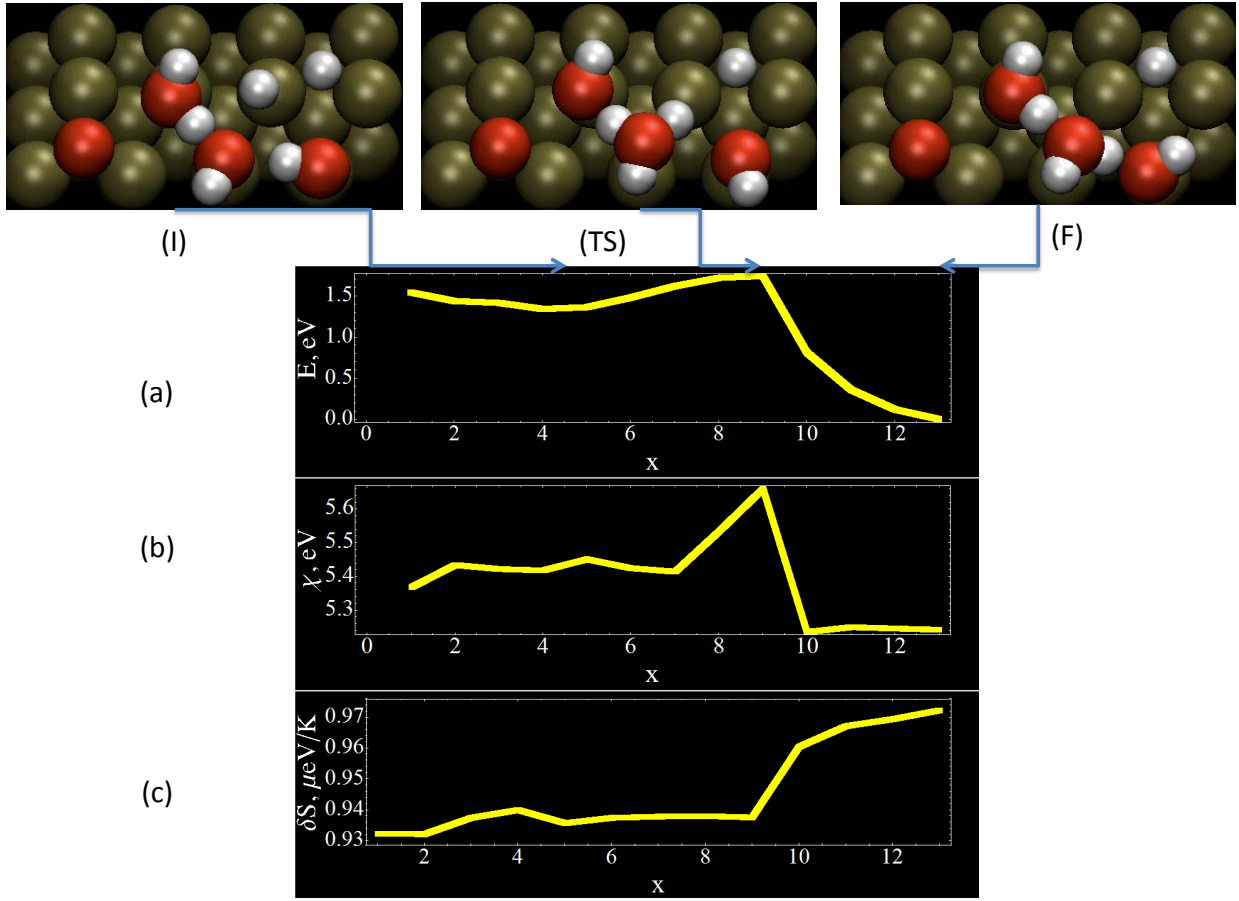


FIG. 11. The change in the energy (a), the workfunction (b), and the electronic delocalization entropy (c) along a minimum reaction path connecting the initial state (I) through the transition state (TS) to the final state (F) for the pathway eq. (6).

REFERENCES

- ¹A. Hervier, J. R. Renzas, J. Y. Park, and G. A. Somorjai, *Nano Lett.* **9**, 3930 (2009).
- ²K. Schierbaum and M. El Achhab, *Phys. Status Solidi A* **208**, 2796 (2011).
- ³H. Nienhaus, *Surf. Sci. Rep.* **45**, 1 (2002).
- ⁴Y. Huang, C. T. Rettner, D. J. Auerbach, and A. M. Wodtke, *Science* **290**, 111 (2000).
- ⁵N. Shenvi, S. Roy, and J. C. Tully, *Science* **326**, 829 (2009).
- ⁶B. Gergen, H. Nienhaus, W. H. Weinberg, and E. W. McFarland, *Science* **294**, 2521 (2001).
- ⁷J. R. Renzas and G. A. Somorjai, *J. Phys. Chem. C* **114**, 17660 (2010).
- ⁸M. A. Hashemian, S. K. Dasari, and E. G. Karpov, *J. Vac. Sci. Technol. A* **31**, 020603 (2013).
- ⁹B. Schindler, D. Diesing, and E. Hasselbrink, *J. Phys. Chem. C* **117**, 6337 (2013).
- ¹⁰H. Nienhaus, H. S. Bergh, B. Gergen, A. Majumdar, W. H. Weinberg, and E. W. McFarland, *Phys. Rev. Lett.* **82**, 446 (1999).
- ¹¹K. Jacobi, ed., *Electron work function of metals and semiconductors*, Landolt-Brnstein - Group III Condensed Matter, Vol. 42A2 (Springer-Verlag, 2005).
- ¹²A. M. Wodtke, D. Matsiev, and D. J. Auerbach, *Prog. Surf. Sci.* **83**, 167 (2008).
- ¹³P. J. Linstrom and W. G. Mallard, eds., *NIST Chemistry WebBook, NIST Standard Reference Database Number 69* (National Institute of Standards and Technology, Gaithersburg MD, 20899, 2013).
- ¹⁴X. Ji, A. Zupperro, J. M. Gidwani, and G. A. Somorjai, *Nano Lett.* **5**, 753 (2005).
- ¹⁵X. Z. Ji and G. A. Somorjai, *J. Phys. Chem. B* **109**, 22530 (2005).
- ¹⁶D. J. Auerbach and A. M. Wodtke, *Dynamics of Gas-Surface Interactions*, edited by R. Dez Muio and H. F. Busnengo, Springer Series in Surface Sciences, Vol. 50 (Springer Berlin Heidelberg, 2013) pp. 267–297.
- ¹⁷G. D. Mahan, *Many-particle physics* (Kluwer Academic/Plenum Publishers, New York, 2000).
- ¹⁸J. W. Gadzuk, *J. Phys. Chem. B* **106**, 8265 (2002).
- ¹⁹J. C. Tully, *Ann. Rev. Phys. Chem.* **51**, 153 (2000).
- ²⁰J. W. Gadzuk and S. Holloway, *Phys. Rev. B* **33**, 4298 (1986).
- ²¹P. Nordlander and J. C. Tully, *Surf. Sci.* **211-212**, 207 (1989).

- ²²M. Head-Gordon and J. C. Tully, J. Chem. Phys. **103**, 10137 (1995).
- ²³J. W. Gadzuk, J. Chem. Phys. **79**, 6341 (1983).
- ²⁴M. Persson and B. Hellsing, Phys. Rev. Lett. **49**, 662 (1982).
- ²⁵V. Krishna and J. C. Tully, J. Chem. Phys. **125**, 054706 (2006).
- ²⁶S. N. Maximoff and M. P. Head-Gordon, Proc. Nat. Acad. Sci. **106**, 11460 (2009).
- ²⁷R. Newton, *Scattering Theory of Waves and Particles*, Dover Books on Physics Series (Dover Publications, 1982).
- ²⁸*Landolt-Börnstein's Numerical Data and Functional Relationships in Science and Technology*, Group III Condensed Matter (Springer-Verlag, 2005).
- ²⁹G. A. Somorjai and Y. Li, *Introduction to Surface Chemistry And Catalysis* (Wiley, 2010).
- ³⁰V. P. Zhukov, E. V. Chulkov, and P. M. Echenique, Phys. Rev. B **73**, 125105 (2006).
- ³¹D. H. Dutton, B. N. Brockhouse, and A. P. Müller, Can. J. Phys. **50**, 2915 (1972).
- ³²M. Reed and B. Simon, *Methods of Modern mathematical physics: Scattering Theory*, Vol. 3 (Academic Press, San Diego, 1979).
- ³³L. D. Faddeev and S. P. Merkuriev, *Quantum Scattering Theory for Several Particle Systems*, Mathematical Physics and Applied Mathematics (Kluwer Academic Publishers, 1993).
- ³⁴J. Y. Park, J. R. Renzas, A. M. Contreras, and G. A. Somorjai, Top. Catal. **46**, 217 (2007).
- ³⁵J. L. Gland, B. A. Sexton, and G. B. Fisher, Surf. Sci. **95**, 587 (1980).
- ³⁶A. C. Luntz, J. Grimblot, and D. E. Fowler, Phys. Rev. B **39**, 12903 (1989).
- ³⁷W. Wurth, J. Stöhr, P. Feulner, X. Pan, K. R. Bauchspiess, Y. Baba, E. Hudel, G. Rocker, and D. Menzel, Phys. Rev. Lett. **65**, 2426 (1990).
- ³⁸C. Puglia, A. Nilsson, B. Hernnäs, O. Karis, P. Bennich, and N. Martensson, Surf. Sci. **342**, 119 (1995).
- ³⁹A. N. Artsyukhovich, V. A. Ukraintsev, and I. Harrison, Surf. Sci. **347**, 303 (1996).
- ⁴⁰H. Steininger, S. Lehwald, and H. Ibach, Surf. Sci. **123**, 1 (1982).
- ⁴¹J. Yoshinobu and M. Kawai, J. Chem. Phys. **103**, 3220 (1995).
- ⁴²A. Eichler and J. Hafner, Phys. Rev. Lett. **79**, 4481 (1997).
- ⁴³A. Groß, A. Eichler, J. Hafner, M. J. Mehl, and D. A. Papaconstantopoulos, J. Chem. Phys. **124**, 174713 (2006).

- ⁴⁴N. Materer, U. Starke, A. Barbieri, R. Dll, K. Heinz, M. V. Hove, and G. A. Somorjai, *Surf. Sci.* **325**, 207 (1995).
- ⁴⁵B. C. Stipe, M. A. Rezaei, and W. Ho, *J. Chem. Phys.* **107**, 6443 (1997).
- ⁴⁶T. Zambelli, J. V. Barth, and G. Ertl, *Nature* **390**, 495 (1997).
- ⁴⁷C. J. Noble, K. Higgins, G. Wöste, P. Duddy, P. G. Burke, P. J. O. Teubner, A. G. Middleton, and M. J. Brunger, *Phys. Rev. Lett.* **76**, 3534 (1996).
- ⁴⁸P. H. Krupenie, *J. Phys. Chem. Ref. Data* **1**, 423 (1972).
- ⁴⁹I. Panas and P. Siegbahn, *Chem. Phys. Lett.* **153**, 458 (1988).
- ⁵⁰J. Ludwig and D. G. Vlachos, *J. Chem. Phys.* **128**, 154708 (2008).
- ⁵¹G. J. Schulz, *Rev. Mod. Phys.* **45**, 423 (1973).
- ⁵²A. Anton and D. C. Cadogan, *Surf. Sci.* **239**, L548 (1990).
- ⁵³W. J. Griffiths and F. M. Harris, *Org. Mass Spectrom.* **22**, 559 (1987).
- ⁵⁴S. Völkening, K. Bedürftig, K. Jacobi, J. Wintterlin, and G. Ertl, *Phys. Rev. Lett.* **83**, 2672 (1999).
- ⁵⁵A. Michaelides and P. Hu, *J. Am. Chem. Soc.* **123**, 4235 (2001).
- ⁵⁶G. B. Fisher and B. A. Sexton, *Phys. Rev. Lett.* **44**, 683 (1980).
- ⁵⁷G. S. Karlberg, G. Wahnstrom, C. Clay, G. Zimbitas, and A. Hodgson, *J. Chem. Phys.* **124**, 204712 (2006).
- ⁵⁸P. Giannozzi, S. Baroni, N. Bonini, M. Calandra, R. Car, C. Cavazzoni, D. Ceresoli, G. L. Chiarotti, M. Cococcioni, I. Dabo, A. Dal Corso, S. de Gironcoli, S. Fabris, G. Fratesi, R. Gebauer, U. Gerstmann, C. Gougoussis, A. Kokalj, M. Lazzeri, L. Martin-Samos, N. Marzari, F. Mauri, R. Mazzarello, S. Paolini, A. Pasquarello, L. Paulatto, C. Sbraccia, S. Scandolo, G. Sclauzero, A. P. Seitsonen, A. Smogunov, P. Umari, and R. M. Wentzcovitch, *J. Phys. Condens. Matter* **21**, 395502 (19pp) (2009).
- ⁵⁹J. P. Perdew, J. A. Chevary, S. H. Vosko, K. A. Jackson, M. R. Pederson, D. J. Singh, and C. Fiolhais, *Phys. Rev. B* **46**, 6671 (1992).
- ⁶⁰G. Mills, H. Jonsson, and G. K. Schenter, *Surf. Sci.* **324**, 305 (1995).
- ⁶¹H. J. Monkhorst and J. D. Pack, *Phys. Rev. B* **13**, 5188 (1976).
- ⁶²M. Methfessel and A. T. Paxton, *Phys. Rev. B* **40**, 3616 (1989).
- ⁶³P. E. Blöchl, O. Jepsen, and O. K. Andersen, *Phys. Rev. B* **49**, 16223 (1994).